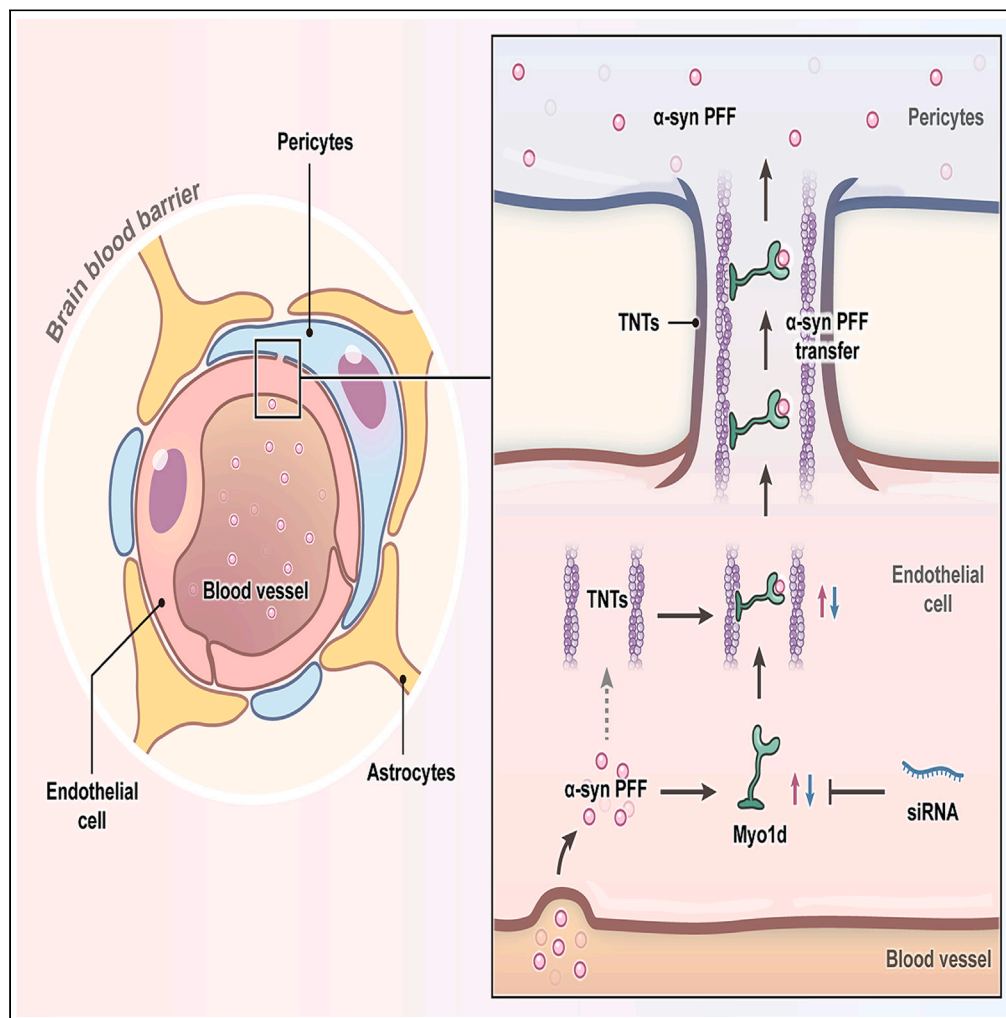# iScience

Article

Myo1d promotes alpha-synuclein transfer from brain microvascular endothelial cells to pericytes through tunneling nanotubes

Qingrui Duan, Qingxi Zhang, Kun Nie, ..., Yuhu Zhang, Yuyuan Gao, Lijuan Wang

gaoyuyuan@gdph.org.cn (Y.G.)
wanglijuan@gdph.org.cn (L.W.)

Highlights

The mechanisms of TNT and Myo1d for α-syn transfer BMVECs-pericytes is proposed

TNTs between BMVECs and pericytes are important for intercellular α-syn spreading

Target Myo1d may be an approach for preventing α-syn spreading BMVECs-pericytes

Article

Myo1d promotes alpha-synuclein transfer from brain microvascular endothelial cells to pericytes through tunneling nanotubes

Qingrui Duan,[1,2,3] Qingxi Zhang,[2,3] Kun Nie,[2,3] Rui Huang,[2,3] Jianhua Yang,[2,3] Peikun He,[2,3] Zihui Tie,[2,3] Haifeng Huang,[2,3] Guixian Ma,[2,3] Yuhu Zhang,[2,3] Yuyuan Gao,[2,3,*] and Lijuan Wang[1,2,3,4,*]

SUMMARY

α-Synuclein preformed fibrils (α-syn PFF) in the blood can cross the blood–brain barrier and invade the central nervous system. Our previous study proved that α-syn PFF can be taken up by brain microvascular endothelial cells (BMVECs). Here, we found that α-syn PFF spread from BMVECs to pericytes with the highest transmission efficiency. We observed abundant tunneling nanotubes (TNTs) connecting BMVECs and pericytes, and α-syn PFF transmitted through these TNTs. Furthermore, α-syn PFF accumulation in BMVECs did not promote TNT formation, but activated the molecular motor Myo1d. Inhibition of Myo1d prevented α-syn PFF transfer from BMVECs to pericytes and decreased the colocalization of Myo1d and F-actin in BMVECs. In summary, we are the first to demonstrate that α-syn PFF spread from BMVECs to pericytes through a mechanism involving TNTs and myosin. Targeting Myo1d may be a promising approach to prevent α-syn spreading from the blood to the brain.

INTRODUCTION

The recent rapid increase in the number of older adults has led to a significant increase in the number of patients with Parkinson's disease (PD).[1] Alpha-synuclein (α-syn) is the key protein implicated in PD etiology.[2,3] α-Syn protofibrils cause the aggregation of endogenous α-syn and neuronal death; additionally, the transfer of misfolded aggregates of α-syn from one brain region to another is implicated in the PD process.[4,5] Pathological α-syn has been considered to exhibit "prion-like" spread throughout the central nervous system (CNS).[6,7] In addition to the intracerebral route, α-syn can be transmitted into the CNS via several routes, including the intraperitoneal, intravenous, and oral routes.[8] The serum levels of α-syn exceed the level in the cerebrospinal fluid (CSF)[9]; however, little research has focused on the role of blood α-syn in PD pathogenesis. Lohmann, S. et al. found that α-syn preformed fibrils (α-syn PFF) can invade the CNS after a single intravenous injection and cause neuropathology and disease in TgM83^{+/−} mice.[10] α-Syn strains can cross the blood–brain barrier (BBB) and invade the CNS when injected into the tail vein of rats.[11] The mechanism underlying the blood-to-brain uptake of α-syn has yet to be defined. Matsumoto, J et al. showed that erythrocyte-derived α-syn-rich extracellular vesicles cross the BBB via adsorptive-mediated transcytosis in the presence of lipopolysaccharide (LPS)-induced systemic inflammation.[12] Normally, α-syn transport from the blood to the brain is controlled by the BBB, and brain microvascular endothelial cells (BMVECs) regulate molecular exchange to maintain CNS homeostasis.[13] However, α-syn can cross the normal mouse BBB in the blood-to-brain direction after intravenous injection.[14] Our previous study proved that BMVECs take up α-syn PFF, exacerbating endothelial damage and promoting cognitive impairment in a mouse model of PD.[15] However, how exogenous α-syn PFF in BMVECs further spreads to the brain has not been elucidated.

The BBB comprises BMVECs surrounded by pericytes and astrocytes.[16–18] Pericytes, the nearest neighbors of BMVECs, play a crucial role in development, regulating permeability and the BBB.[19,20] Astrocytic endfeet cover BMVECs and control brain water permeability with a unique aquaporin-4 (AQP4) water channel.[21] Recognizing this association between BMVECs with pericytes and astrocytes, we designed coculture models, including BMVECs-to-BMVECs (B-B), BMVECs-to-pericytes (B-P) and BMVECs-to-astrocytes (B-A), to compare the transmission efficiency of α-syn PFF in BMVECs, highlighting the direction of spreading of α-syn PFF in BMVECs to the brain. Our results show that α-syn PFF transmitted from BMVECs to pericytes

[1]School of Medicine, South China University of Technology, Guangzhou 510006, China

[2]Department of Neurology, Guangdong Neuroscience Institute, Guangdong Provincial People's Hospital (Guangdong Academy of Medical Sciences), Southern Medical University, Guangzhou 510080, China

[3]Guangzhou Key Laboratory of Diagnosis and Treatment for Neurodegenerative Diseases, Guangdong Provincial People's Hospital (Guangdong Academy of Medical Sciences), Southern Medical University, Guangzhou 510080, China

[4]Lead contact

*Correspondence:
gaoyuyuan@gdph.org.cn (Y.G.),
wanglijuan@gdph.org.cn (L.W.)
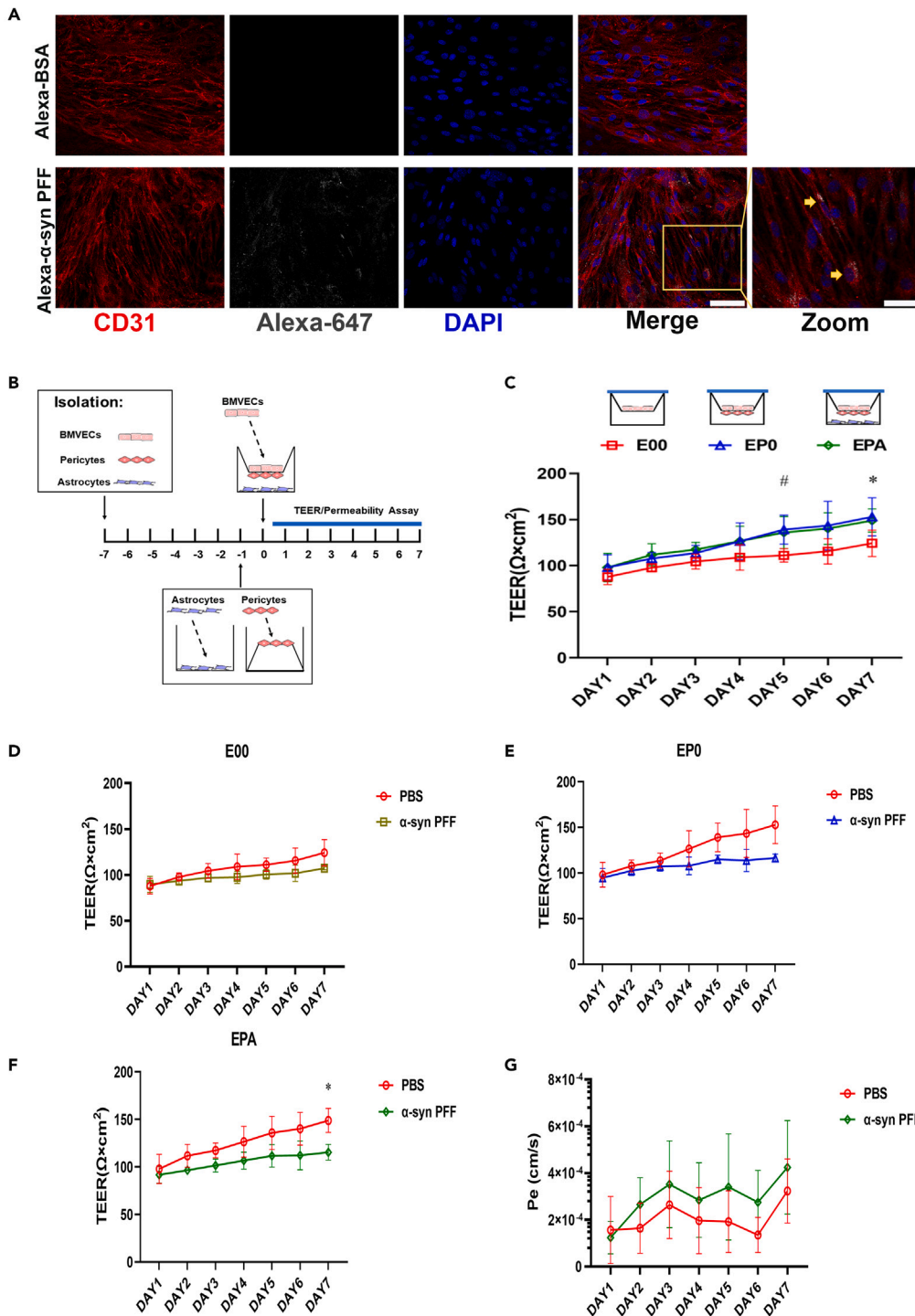https://doi.org/10.1016/j.isci.2023.107458

Figure 1. Entry of exogenous α-syn PFF into BMVECs damaged barrier function

(A) Alexa 647 Protein Labeling Kits stained BSA and α-syn PFF (Alexa-BSA was used as a negative control), then treated BMVECs for 24 h individually. Representative images of the two groups co-immunostained with CD31 (red), Alexa 647 signal (white). The magnification view of zoom was displayed, and the yellow arrows indicated the internalized Alexa-α-syn PFF. Nuclei were stained with DAPI (blue). Scale bar = 57.9μm or 28.9μm.

(B) Schematic diagram of the preparation of the *in vitro* BBB model.

Figure 1. Continued

(C) TEER values of the different BBB models constructed from BMVECs (E), pericytes (P) and astrocytes (A) on days 1–7. # symbol represents statistically significant differences (p < 0.05) in TEER of EP0 compared with E00, * symbol represents statistically significant differences (p < 0.05) in TEER of EPA compared with E00. n = 5.

(D–F) TEER value of the E00 model (D), the EP0 model (E), the EPA model (F) with PBS or α-syn PFF treatment on days 1–7. n = 5.

(G) Endothelial permeability coefficient for FD40 in the EPA model on days 1–7. n = 5. All data are presented as mean ± SD. *p < 0.05. Two-Way Repeated-Measures ANOVA with Tukey's test.

with the highest efficiency. Several transfer mechanisms have been considered, including exocytosis/endocytosis, extracellular vesicle secretion, and prion-like spreading; however, many questions remain regarding how α-syn PFF in BMVECs spreads to pericytes.

Tunneling nanotubes (TNTs) are thin, long F-actin-based membranous channels that allow direct physical connections between different cells and transfer cellular components such as organelles, ions, small molecules and proteins.[22] TNTs have been shown to act as channels for α-syn transfer in various cell types, including neurons, astrocytes, and pericytes.[23–25] TNT formation arises from the extension of filopodia-like protrusions toward neighboring cells.[26,27] Errede, M. et al. found that TNTs evoked communication between pericytes and endothelial cells during normal angiogenesis.[28] Here, we detected that the α-syn PFF in BMVECs can be transmitted to pericytes by B-P TNT connections. However, the mechanism of α-syn PFF transfer via B-P TNTs remains unclear.

Molecular motors, including the kinesin, dynein, and myosin superfamilies have been found to transport cellular components. Myosin proteins bind to actin and move along actin filaments by ATP hydrolysis.[29] Myosin-X (Myo10), an unconventional myosin, is involved in filopodia and TNT formation.[30] Kinesins and dyneins move along microtubules. Their motor domain binds to microtubules, allowing movement through ATP hydrolysis.[31] We compared BMVECs with or without α-syn PFF treatment using RNA-seq to examine the α-syn PFF transfer mechanism and identified Myo1d as a key molecule in this process. Myo1d is localized in F-actin and involved in endocytic membrane trafficking.[32] Therefore, we hypothesize that exogenous α-syn PFF internalized by BMVECs can be further transmitted to pericytes by B-P TNTs and that this process may involve α-syn PFF-mediated promotion of Myo1d expression.

RESULTS

Entry of exogenous α-syn PFF into BMVECs damaged barrier function

We produced α-syn PFF and determined the amyloid fibril structure (Figure S1). In BMVECs treated with exogenous α-syn PFF, α-syn PFF could be taken up by endothelial cells and aggregated in cells (Figure 1A). Then, we investigated the effects of α-syn PFF on endothelial and barrier function. To construct *in vitro* BBB models, we isolated primary BMVECs, pericytes and astrocytes, and verified them by immunostaining (Figure S2). We established three *in vitro* BBB models to assess barrier function: endothelial monocultures (E00), cocultures of endothelial cells with pericytes (EP0), and tricultures of endothelial cells with pericytes and astrocytes (EPA) (Figure 1B). The TEER values of the EP0 group on day 5 and the EPA group on day 7 were significantly increased compared with that of the endothelial monoculture, but the TEER value was not significantly different between the coculture and triculture groups (Figure 1C). Compared with the control group, the TEER values of α-syn PFF-treated BMVECs were decreased in the three models, but only the EPA group significantly differed at day 7 (Figures 1D–1F). In the EPA model, permeability was increased after α-syn PFF treatment; however, the permeability was not significantly different between α-syn PFF-treated group and control group (Figure 1G).

α-Syn PFF transmitted from BMVECs to pericytes with the highest efficiency

To confirm the spreading direction of α-syn PFF in BMVECs, we designed coculture models, BMVECs-to-BMVECs (B-B), BMVECs-to-pericytes (B-P) and BMVECs-to-astrocytes (B-A), representing the association between BMVECs and pericytes and astrocytes (Figure 2A). Then, we compared the transmission efficiency among the three groups, and found that α-syn PFF transmitted with the highest efficiency in the B-P model (mean = 76.01%), the middle efficiency in the B-B model (mean = 54.69%), and the lowest efficiency in the B-A model (mean = 31.28%) (Figures 2B and 2C). Therefore, the spreading direction of α-syn PFF in BMVECs was found to be more inclined toward pericytes.

Next, we further detected the best time and conditions for the transmission from BMVECs to pericytes. The highest transmission efficiency in the B-P model was observed on day3, and extending the coculture time
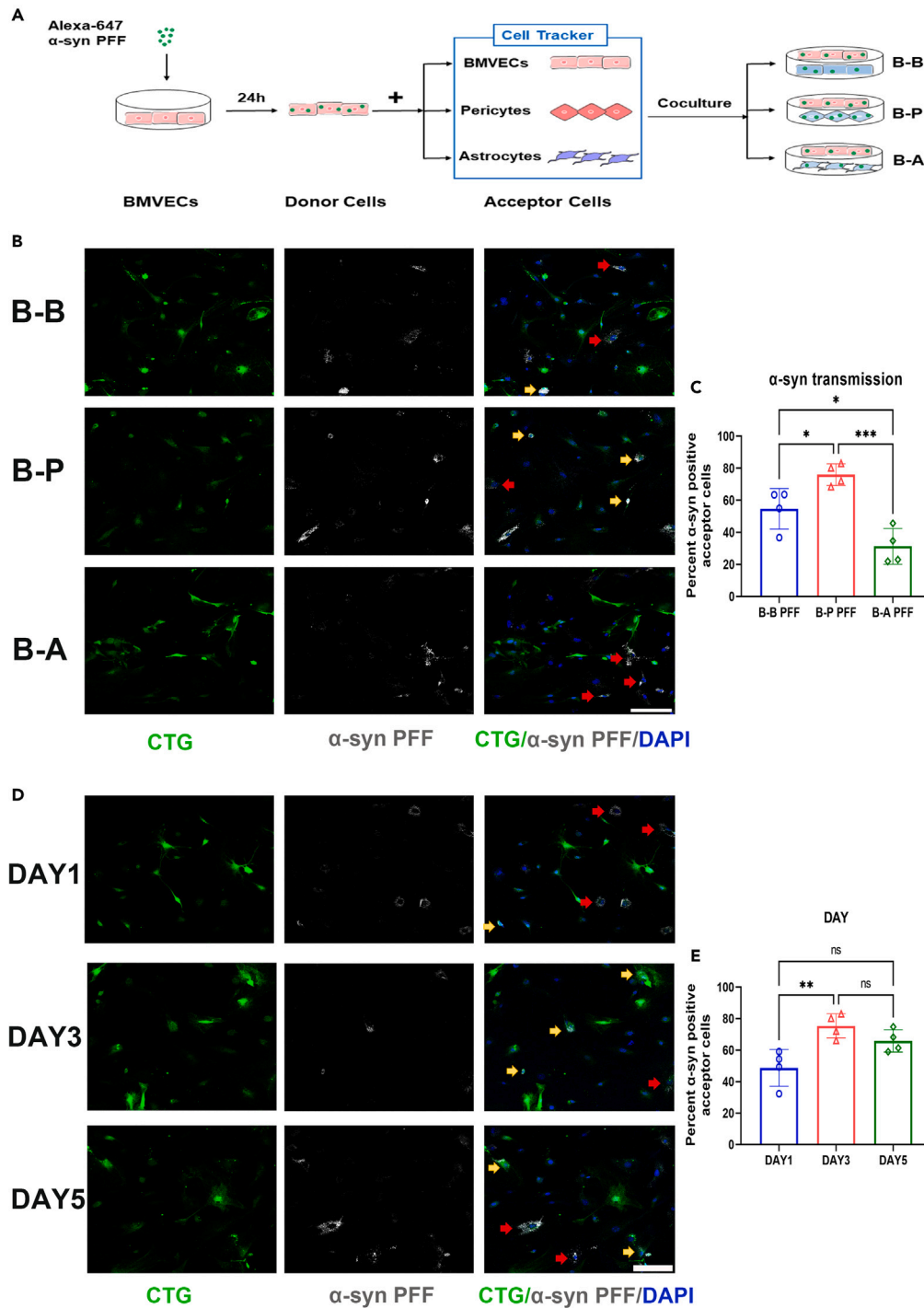
Figure 2. α-Syn PFF in BMVECs has the highest transmission efficiency to pericytes

(A) Schematic diagram of the coculture models reflecting α-syn PFF transfer, BMVECs-to-BMVECs (B-B), BMVECs-to-pericytes (B-P) and BMVECs-to-astrocytes (B-A).

(B) Representative images of α-syn PFF spreading the three coculture models. n = 4 independent tests with 170–240 individual cells.

(C) Percent of α-syn positive acceptor cells was presented as the transmitted efficiency in the three groups.

(D) Representative images of α-syn PFF spreading from BMVECs to pericytes on days 1, 3, and 5.

Figure 2. *Continued*

(E) Percent of α-syn positive acceptor cells was presented as the transmitted efficiency of α-syn PFF on days 1, 3, and 5. n = 4 independent tests with 170–240 individual cells. CellTracker Green (CTG) stained acceptor cells, and the yellow and red arrows individually indicated spreading or no spreading to acceptor cells. Nuclei were stained with DAPI (blue). Scale bar = 115.8μm. Data are presented as mean ± SD. *p < 0.05, **p < 0.01, ***p < 0.001. One-way ANOVA with Tukey's multiple comparison.

did not further enhance the transmission efficiency (Figures 2D and 2E). Incidentally, we found that the transmission efficiency of α-syn PFF from BMVECs to pericytes decreased significantly in low-glucose culture conditions (Figure S3), indicating that the process of α-syn PFF transfer requires energy consumption.

α-Syn PFF transmission from BMVECs to pericytes through TNTs

TNTs, direct cell-to-cell contacts, could facilitate the intercellular transmission of pathogenic proteins. To confirm whether TNTs contact BMVECs with pericytes, we stained the acceptor cells (pericytes) and the plasma membrane with WGA. TNTs were frequently formed between BMVECs and pericytes in normal coculture at day 3 (Figure 3A). We used α-syn PFF-treated BMVECs cocultured with pericytes, and observed fluorescently labeled α-syn PFF in TNTs between BMVECs and pericytes (Figure 3B). Then, we used confocal images and 3D reconstruction to show TNTs between BMVECs and pericytes and demonstrated the localization of α-syn PFF-labeled fluorescence and TNTs (Figure 3C). To further display TNT-mediated α-syn PFF transfer, we performed time-lapse experiments by live imaging, allowing the visualization of TNTs by confocal microscopy. Time-lapse recordings revealed the transfer of α-syn PFF from BMVECs to pericytes via TNTs (Figures 3D and 3E): One was characterized by short TNT connections, which α-syn PFF transferred from BMVECs to pericytes (Figure 3E; Video S1). These results showed that α-syn PFF could transfer from α-syn PFF to pericytes through TNTs.

To confirm the important role of TNT connections, we used latrunculin B to inhibit actin polymerization and significantly reduced the number of TNTs between BMVECs and pericytes (Figures 4A and 4C). We used CellTracker Green to stain pericytes and detected the transmission efficiency in B-P, demonstrating that α-syn PFF transmission was significantly reduced after latrunculin B treatment (Figure 4A). Moreover, pericytes were labeled with PDGFR-β to assess the transmission efficiency in the B-P model, and α-syn PFF transmission in the latrunculin B-treated group was obviously decreased compared with that in the α-syn PFF-treated group (Figure 4B). The transmission efficiency of α-syn PFF decreased by nearly half (mean = 40.16%, p value < 0.001) after inhibition of TNT formation (Figure 4D). However, we cannot exclude the possibility that other transfer pathways contribute to α-syn PFF transmission from BMVECs to pericytes. Overall, these results demonstrate that TNT connections are important for α-syn PFF transfer between BMVECs and pericytes.

α-Syn PFF accumulation in BMVECs could not promote TNT formation but activated the molecular motor Myo1d

To identify whether the high load of intracellular α-syn PFF affected the formation of TNTs between BMVECs and pericytes, we investigated the total number of TNT connections in cultures treated or untreated with α-syn PFF. Our results showed that α-syn PFF exposure did not significantly increase TNT formation (Figures 5A and 5B), indicating that α-syn PFF accumulation in BMVECs cannot promote TNT formation. However, the inhibition of TNTs by latrunculin B can significantly reduce the transmission efficiency of α-syn PFF between BMVECs and pericytes.

TNTs are F-actin-based membranous channels; thus, we investigated whether myosin proteins that bind to actin and move along actin filaments by ATP hydrolysis can combine with TNTs and promote α-syn PFF transfer. We screened the key molecules of myosin proteins using RNA-seq by comparing BMVECs with or without α-syn PFF treatment. There were 1297 differentially expressed genes (DEGs) identified using DESeq2, with log2(FC) > 1 or < −1 and Q value ≤0.05; 378 genes were upregulated, and 919 were downregulated (Figure 6A). The expression patterns of the top 20 upregulated and downregulated DEGs are shown in the heatmap (Figure S4A). Then, we analyzed GO terms based on DEGs to obtain functional annotations of biological processes. Our results showed that the 378 upregulated DEGs were mainly enriched in terms related two aspects: the extracellular space and the plasma membrane. Specifically, they were enriched in the plasma membrane integral component of plasm (GO:0005887), plasma membrane (GO:0005886) and cell surface (GO:0009986), which is consistent with the characteristic of TNTs as
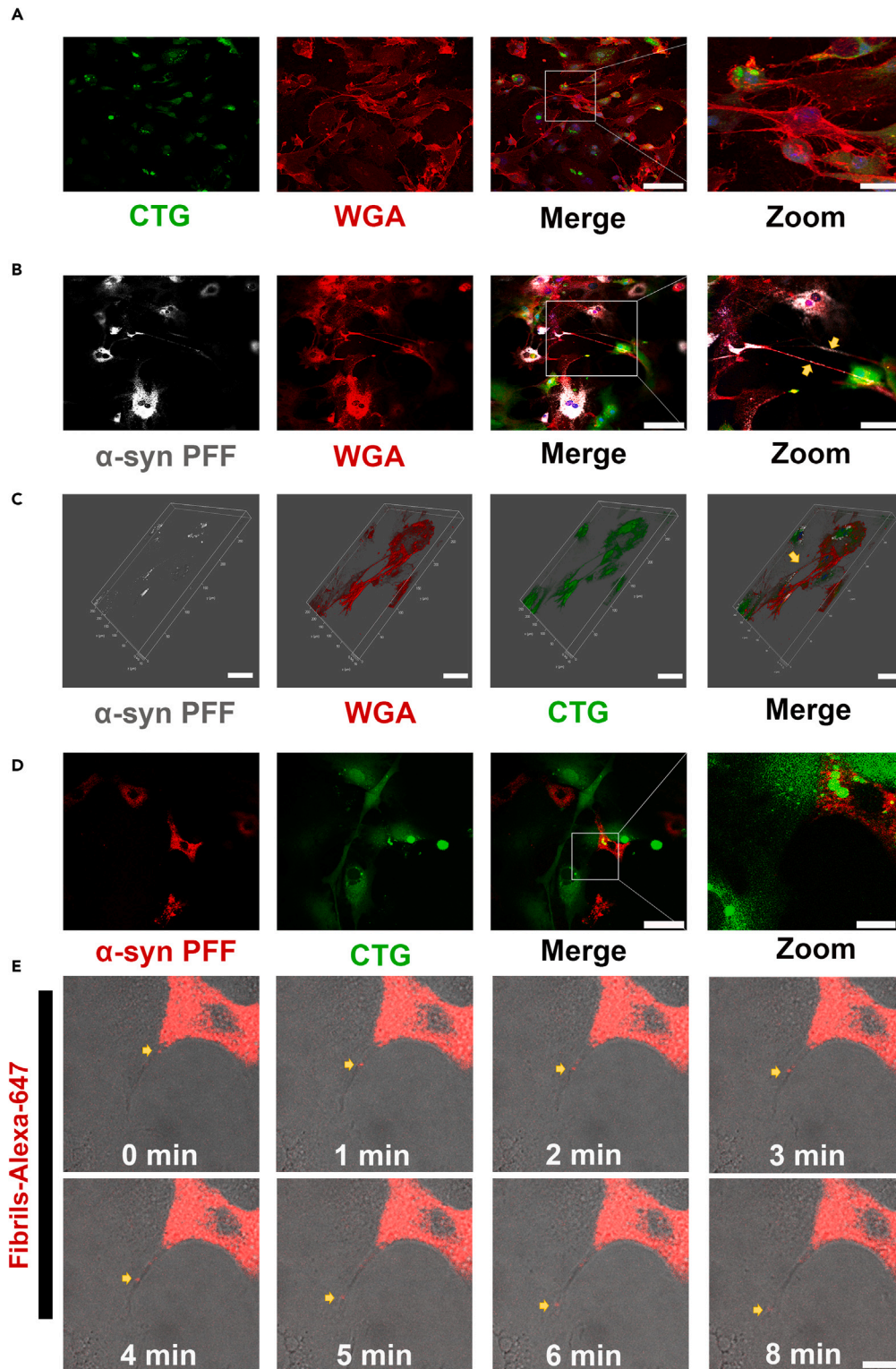
Figure 3. α-Syn PFF transmission from BMVECs to pericytes through TNTs connections
(A) Representative images of TNTs connections between BMVECs and pericytes in normal coculture at day 3. CTG (green) stained acceptor cells (pericytes), membrane staining using WGA (red) showed TNTs. Scale bar = 115.8μm or 28.9μm.
(B) Representative images of α-syn PFF-treated BMVECs coculture with pericytes through TNTs, and the yellow arrows indicated the continuous white dots (Alexa-α-syn PFF) distributed along TNTs (WGA) connections between BMVECs and pericytes. Scale bar = 115.8μm or 57.9μm.
(C) Representative 3D images of α-syn PFF spreading in the TNTs between BMVECs and pericytes. Scale bar = 50μm.
(D) Pericytes were labeled with CTG (green) and BMVECs treated with Alexa-α-syn PFF (red), which confirmed the direction of α-syn PFF spreading between BMVECs and pericytes in time-lapse recording. Scale bar = 115.8μm or 14.5μm.
(E) Representative time-lapse recording demonstrating the transfer of Alexa-α-syn PFF (red) from BMVECs to pericytes. Nuclei were stained with DAPI (blue). Scale bar = 14.5μm.

membranous channels (Figure S4B); these results were similar to those of the GO analysis of the total DEGs (Figure 6B). Next, we screened myosin proteins in the three GO terms and found myosin regulatory light chain interacting protein (MYLIP) and Myo1d. However, the expression of MYLIP was low and downregulated, and Myo1d was high and upregulated in the α-syn PFF-treated group (Figure S4C). We also analyzed the DEGs in molecular motors, including kinesin, dynein, and myosin, which have been identified to transport cellular components. Myo1d was again found to be upregulated in the α-syn PFF-treated group (Figure 6C). Furthermore, we confirmed the increased expression of Myo1d in BMVECs treated with α-syn PFF using quantitative real-time PCR and western blotting. Our results showed that both the mRNA and protein levels of Myo1d were significantly enhanced in the α-syn PFF- treated group compared with those in the PBS control group (Figures 6D–6F). Overall, these results suggest that α-syn PFF accumulation in BMVECs cannot promote TNT formation but activates the molecular motor Myo1d.

Inhibition of Myo1d could reduce the α-syn PFF transmission from BMVECs to pericytes

Since exposure to α-syn PFF can induce the upregulation of Myo1d in BMVECs, we hypothesized that the activation of Myo1d can induce α-syn PFF transmission from BMVECs to pericytes. To confirm this hypothesis, BMVECs were transfected with Myo1d siRNA to inhibit the expression of Myo1d protein, and the cells were then treated with α-syn PFF. Myo1d levels were significantly decreased in the Myo1d siRNA + PBS and Myo1d siRNA + α-syn PFF groups compared with those in the α-syn PFF groups (Figures 7A and 7B). Next, we used coculture experiments to evaluate the transmission efficiency of α-syn PFF after Myo1d siRNA treatment. Inhibiting Myo1d significantly reduced α-syn PFF transmission from BMVECs to pericytes, decreasing and the transmission efficiency to 35.13% (Figures 7C and 7D). This finding indicates that Myo1d expression modulates intracellular α-syn PFF, which induces intercellular transfer of α-syn PFF.

Localization of Myo1d in F-actin-rich protrusions indicated that Myo1d may mediate α-syn PFF transfer through BMVECs-pericytes TNTs

We have already confirmed that inhibiting Myo1d expression decreases α-syn PFF transfer. To further investigate whether Myo1d combines with TNTs and promotes α-syn PFF transfer, we stained coculture BMVECs and pericyte for Myo1d and F-actin and analyzed the colocalization coefficient of Myo1d and F-actin. The α-syn PFF-treated group demonstrated significantly increased Myo1d and F-actin colocalization in the pseudopodia compared with that in the control (PBS-treated) group. Furthermore, the Myo1d siRNA group with or without α-syn PFF treatment displayed diminished colocalization with F-actin in the pseudopodia (Figures 8A and 8B). These results indicate that Myo1d strongly colocalizes with F-actin, and is crucial in mediating α-syn PFF transfer through BMVECs-pericyte TNTs.

DISCUSSION

The transfer of misfolded aggregates of α-syn to brain regions is implicated in the disease process of PD. A previous study revealed that serum α-syn PFF can invade the CNS, aggravating neuropathology and disease.[10,11] Our previous research confirmed that α-syn PFFs were taken up by BMVECs and exacerbated endothelial damage, promoting cognitive impairment in a mouse model of PD.[15] Therefore, in this study, we revealed the direction and vascular mechanism of α-syn PFF transfer to highlight the underlying mechanism by which α-syn PFF in BMVECs spread to the brain.

Increasing evidence has demonstrated the exchange of α-syn between the brain and peripheral tissues, and α-syn monomers, oligomers and preformed fibrils are internalized and transported by brain endothelial cells, indicating that the trafficking of α-syn in brain endothelial cells plays a crucial role in α-syn spreading between the brain and the periphery.[15,33] Interestingly, α-syn is expressed in and secreted
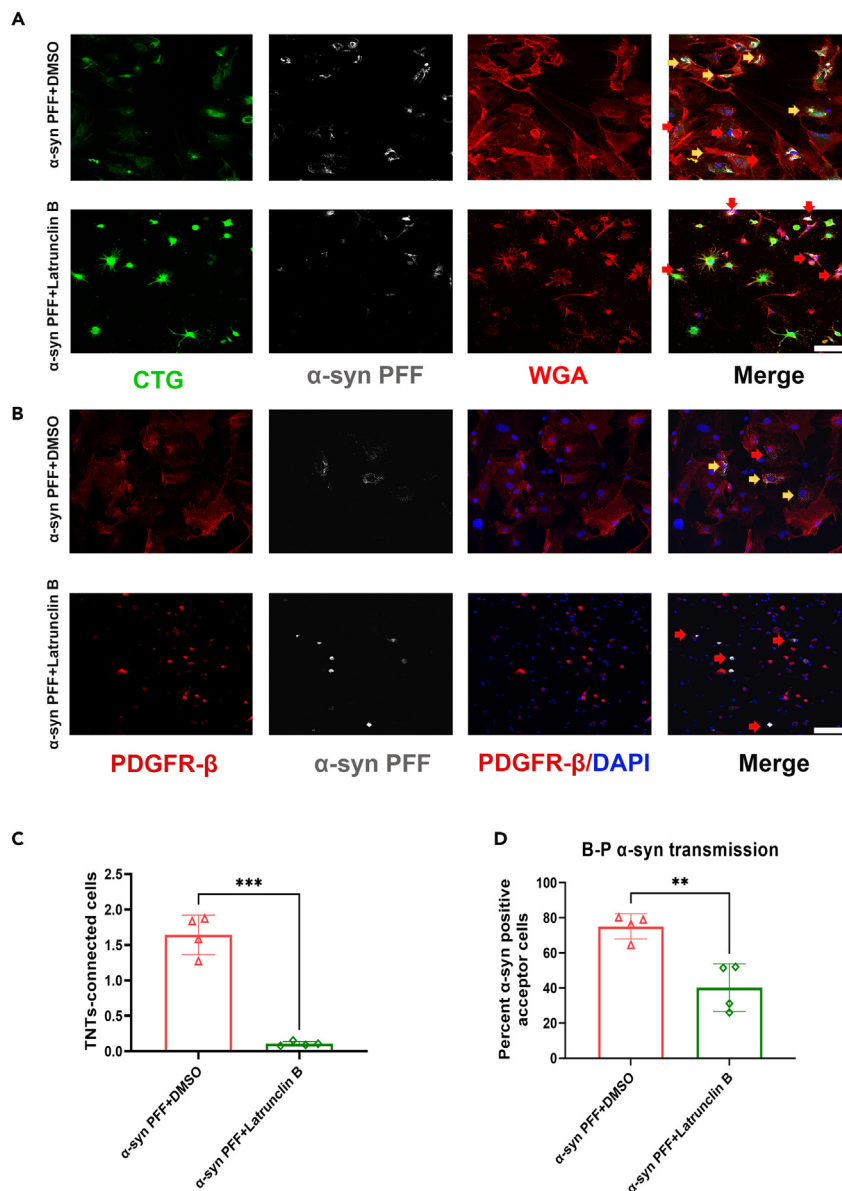
Figure 4. Inhibition of TNTs decreased the α-syn PFF transmission from BMVECs to pericytes

(A) Representative images of α-syn PFF treatment with or without Latrunculin B in the coculture system of BMVECs to pericytes. Alexa 647 Protein Labeling Kits stained α-syn PFF (white), CTG (green) stained acceptor cells (pericytes), membrane staining using WGA (red) showed TNTs.

(B) PDGFR-β (red) stained pericytes and detected transmitted efficiency of α-syn PFF with or without Latrunculin B. The yellow and red arrows individually indicated spreading or no spreading to acceptor cells. Nuclei were stained with DAPI (blue). Scale bar = 115.8μm.

(C) TNTs-connected cells were presented as the number of TNTs. n = 4 independent tests 180–250 individual cells.

(D) Percent of α-syn positive acceptor cells was presented as the transmitted efficiency of α-syn PFF. n = 4 independent tests with 170–240 individual cells. Data are presented as mean ± SD. *p < 0.05, **p < 0.01, ***p < 0.001. Student's t test.

from brain endothelial cells, and endogenous α-syn in endothelial cells might maintain endothelial function.[34] Kuan, W.L. et al. found that α-syn PFF impaired tight junction protein expression but failed to detect a change in TEER values in hCMEC/D3 cells in the upper compartment.[35] These results were consistent with our previous findings.[15] However, both previous studies investigated endothelial function using endothelial cell monolayers in the upper compartment, and the BBB model *in vitro* requires the coculture of endothelial cells, pericytes and astrocytes to mimic the anatomical situation *in vivo*.[19] Here, we showed that
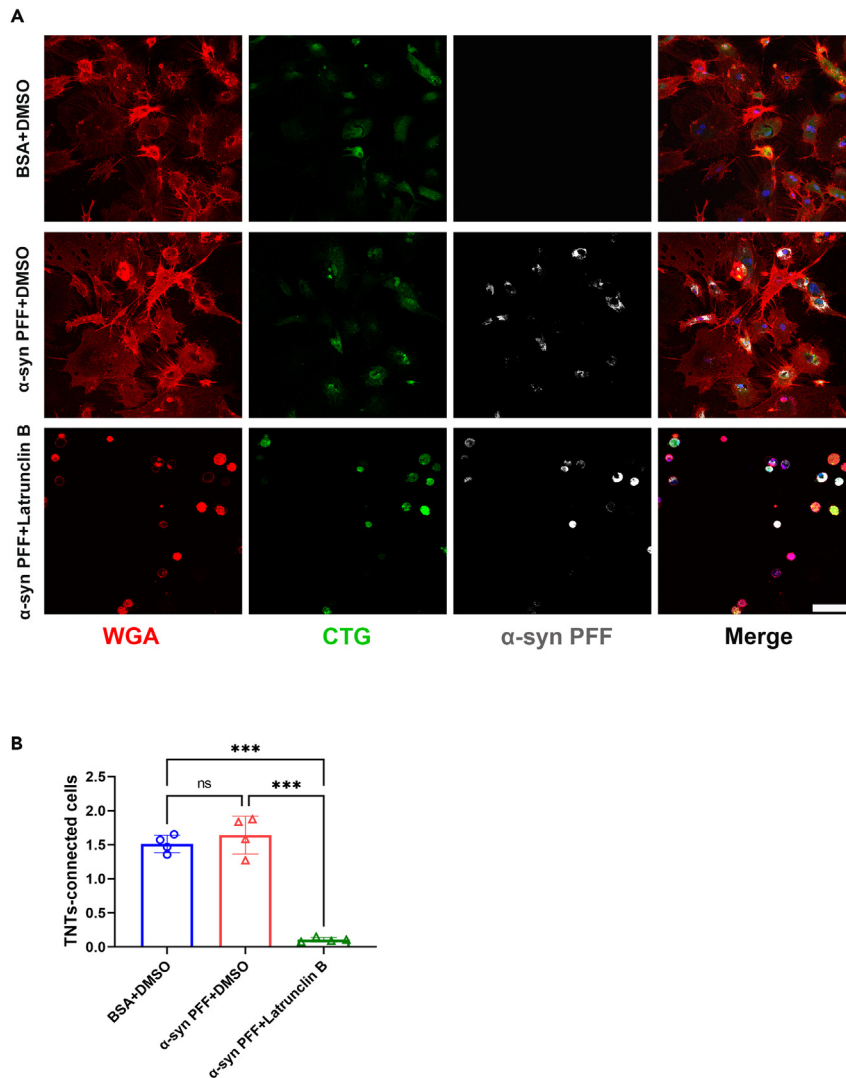
A

B

Figure 5. α-Syn PFF accumulation in BMVECs cannot promote TNTs formation

(A) Representative images of BSA, α-syn PFF, α-syn PFF+Latrunculin B in the coculture system of BMVECs to pericytes. Alexa 647 Protein Labeling Kits stained BSA or α-syn PFF (white), CTG (green) stained acceptor cells (pericytes), membrane staining using WGA (red) showed TNTs. Nuclei were stained with DAPI (blue). Scale bar = 115.8μm.

(B) Percent of α-syn positive acceptor cells was presented as the transmitted efficiency of α-syn PFF. n = 4 independent tests 180–250 individual cells. Data are presented as mean ± SD. *p < 0.05, **p < 0.01, ***p < 0.001. One-way ANOVA with Bonferroni.

exogenous α-syn PFF can be taken up by BMVECs. We subsequently detected endothelial function using three BBB models. The TEER values were higher in double (EP0) and triple (EPA) coculture models than in the endothelial cell monoculture (E00). Treatment of BMVECs with α-syn PFF reduced the TEER values of the three BBB models, but the decrease was significant for only the triple coculture (EPA) model. The triple coculture EPA model showed the tightest paracellular barrier and expressed the highest level of tight junction proteins among the seven models tested in our experiments compared with brain endothelial cells cultured alone.[19] Accordingly, we purport that the triple coculture model EPA is a more sensitive and efficient model for studying the effect of α-syn PFF treatment than the monoculture and double coculture models. However, we could not detect significant impairment of barrier permeability by exogenous α-syn PFF in the triple coculture (EPA) model. Kuan, W.L. showed that there was no significant difference in permeability with or without α-syn PFF treatment in a triple coculture system (hCMEC/D3 cells, primary rodent astrocytes and primary fetal human cortical cells).[35] We speculate that exogenous α-syn PFF into
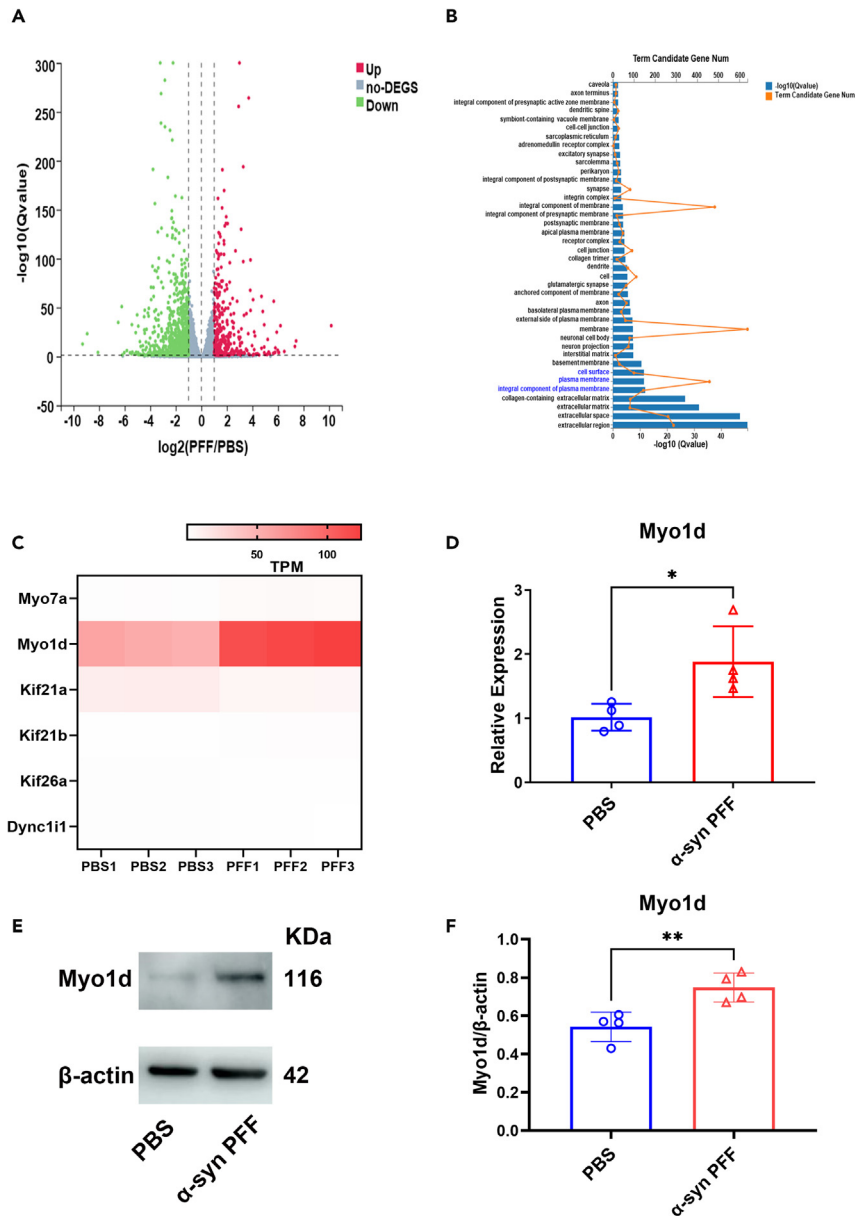
Figure 6. α-Syn PFF accumulation in BMVECs activate molecular motors Myo1d

(A) Total RNA extracted from BMVECs of PBS and α-syn PFF was analyzed using RNA-seq. Volcano plots of all the identified genes in the RNA-seq with upregulated DEGs in red, downregulated DEGs in green, and non-DEGs in gray.

(B) The top 40 of GO functional annotation based on the total DEGs.

(C) Heatmap showed the DEGs expression of molecular motors.

(D) Quantitative PCR analysis of mRNA levels of Myo1d. n = 4.

(E and F) Western blot analysis of protein levels of Myo1d in BMVECs with or without α-syn PFF treatment. β-actin served as a control. n = 4. Data are presented as mean $\pm$ SD. *p < 0.05, **p < 0.01, ***p < 0.001. Student's *t* test.

BMVECs cannot disrupt the expression of tight junctions after 7 days. Tight junctions regulate paracellular permeability and maintain cell polarity.[36,37] Kuan, W.L. also found that α-syn PFF did not significantly alter the expression of claudin-5, an integral membrane tight protein modulating paracellular permeability, after 14 days.

Another study demonstrated transcytosis of monomeric α-syn in the luminal-abluminal direction, suggesting polarized trafficking of monomeric α-syn across the BBB endothelium.[33] However, the transmission
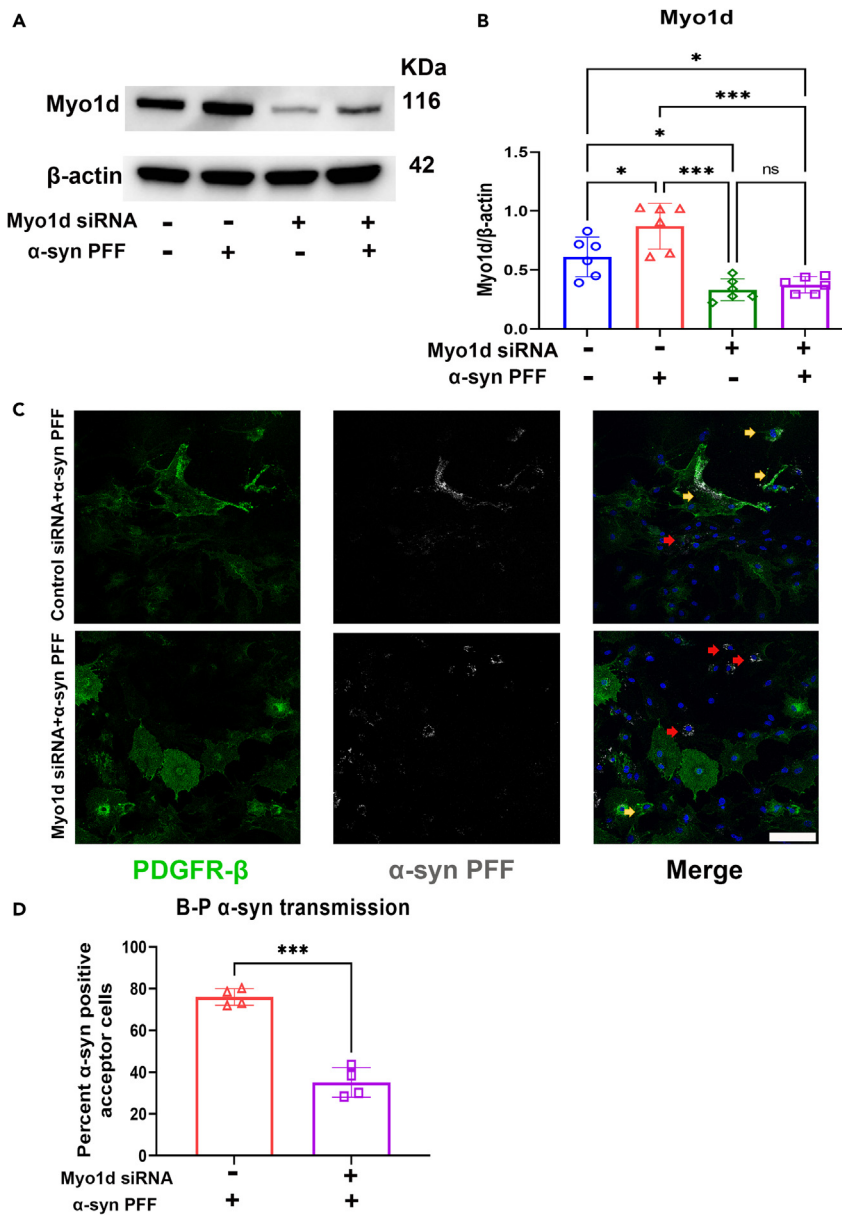
Figure 7. Inhibition of Myo1d can reduce the α-syn PFF transmission from BMVECs to pericytes

(A and B) Western blot analysis of protein levels of Myo1d in primary BMVECs of control siRNA and Myo1d siRNA with or without α-syn PFF treatment. β-actin served as a control. n = 6.

(C) Representative images of α-syn PFF treatment with control siRNA and Myo1d siRNA in the coculture system of BMVECs to pericytes. Alexa 647 Protein Labeling Kits stained α-syn PFF (white), PDGFR-β(green) stained acceptor cells (pericytes), and the yellow and red arrows individually indicated spreading or no spreading to acceptor cells. Nuclei were stained with DAPI (blue). Scale bar = 115.8μm.

(D) Percent of α-syn positive acceptor cells was presented as the transmitted efficiency of α-syn PFF. n = 4 independent tests with 170–240 individual cells. Data are presented as mean ± SD. *p < 0.05, **p < 0.01, ***p < 0.001. One-way ANOVA with Bonferroni (B), Student's t test (D).

route of α-syn PFF from brain endothelial cells is unclear. The BBB is composed of brain endothelial cells surrounded by pericytes and astrocytes, and crosstalk mechanisms between endothelial cells, pericytes, and astrocytes preserve barrier integrity and function under physiological conditions.[38,39] Brain endothelial cells interact with pericytes, astrocytes or blood vessels through exocytosis and direct transfer of cytoplasmic components and proteins.[40–42] Here, we showed that the spreading direction of α-syn PFF in
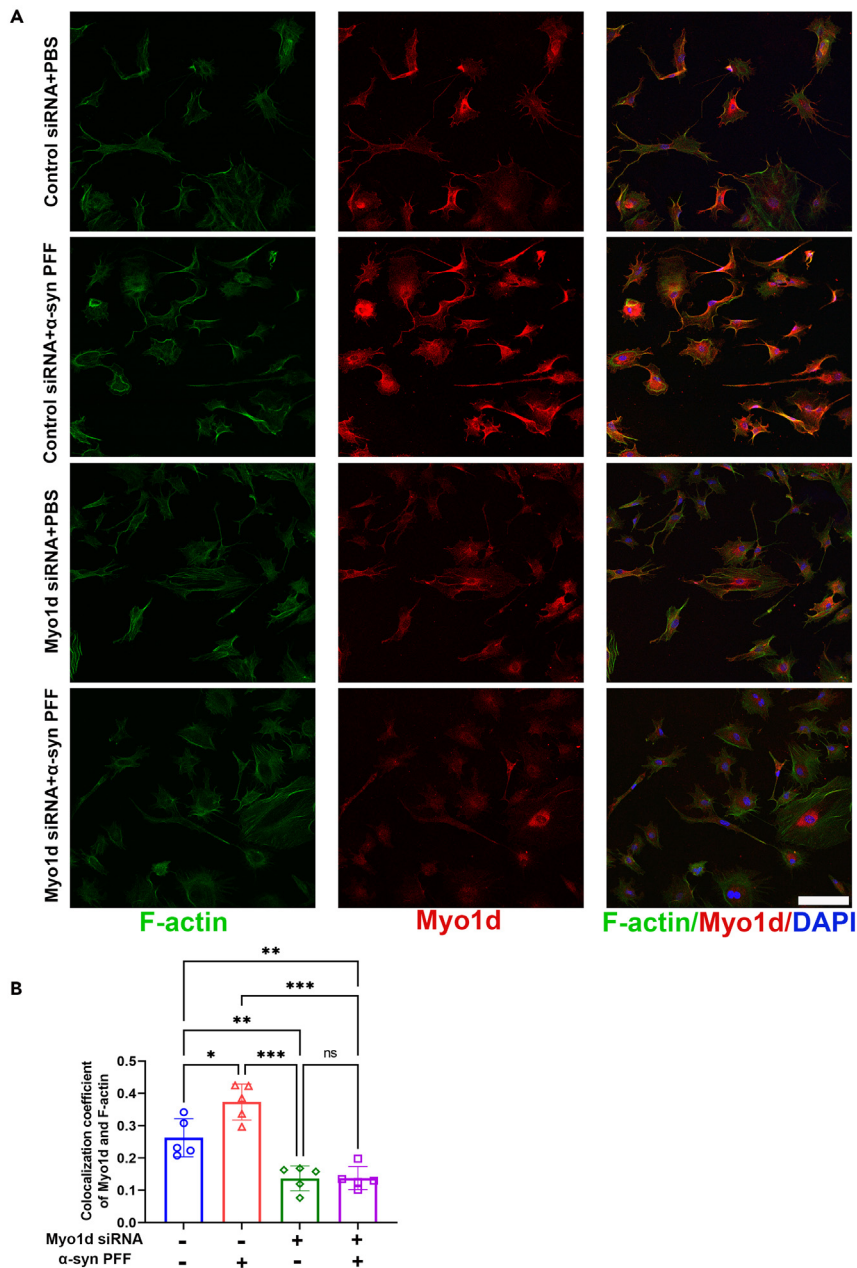
Figure 8. Myo1d localized in F-actin-rich protrusions

(A) Representative images of BMVECs of control siRNA and Myo1d siRNA with or without α-syn PFF treatment. F-actin labeled using phalloidin (green). Nuclei were stained with DAPI (blue). Scale bar = 115.8μm.

(B) Colocalization coefficient of Myo1d and F-actin in BMVECs of control and Myo1d siRNA with or without α-syn PFF treatment. n = 5. Data are presented as mean $\pm$ SD. $*p < 0.05$, $**p < 0.01$, $***p < 0.001$. One-way ANOVA with Bonferroni.

BMVECs was more inclined toward pericytes than toward endothelial cells and astrocytes. Recent evidence has shown that pericytes in the human brain contain α-syn, which is degraded through the lysosomal pathway, suggesting that the accumulation of α-syn in pericytes may play a role in PD pathogenesis.[43] In response to α-syn, pericytes release inflammatory cytokines and matrix metalloproteinase-9 (MMP-9) contributing to BBB breakdown.[44] However, the role of pericytes in the disease processes of PD is poorly understood. This study is the first to demonstrate that the main spreading direction of α-syn PFF in BMVECs mainly spread to pericytes, providing a new target pathway for α-syn PFF transfer. Accordingly, future studies should investigate the role and mechanisms of pericytes in PD pathogenesis.

Regarding intercellular communication, endothelial cells can connect with other cells such as endothelial cells, pericytes, and astrocytes, through TNTs.[28,41,42,45] TNTs originate between two connected cells and contribute to the intercellular spread of components or signals (ions, proteins and organelles).[46] Several studies have shown α-syn PFF transfer between neural and glial cells through TNTs, which may mediate the progression of synucleinopathies.[25,47,48] However, it is unclear whether α-syn PFF in BMVECs can be transmitted to pericytes through TNTs between BMVECs and pericytes. Hence, we designed a coculture model and revealed that α-syn PFF transferred from BMVECs to pericytes via TNTs. This transfer can be decreased by approximately 50% by inhibiting TNT formation using latrunculin B. However, there was still some α-syn PFF transmission from BMVECs to pericytes after latrunculin B treatment. We considered that other spreading mechanisms may mediate α-syn spreading between endothelial cells and pericytes. The mechanisms of cell-to-cell transmission of pathogenic α-syn include exocytosis and endocytosis, uptake of exosomes carrying α-syn, or direct penetration.[47] To further characterize α-syn PFF intercellular traffic, we used cocultures in which BMVECs and pericytes either built direct cell-cell contacts or cocultures separated by transwell membranes (pore size 8.0 μm). We could not detect α-syn PFF-positive in pericytes when cells were cocultured without direct contact (data not shown). The results were consistent with Scheiblich, H. et al. findings that *α-syn*-positive acceptors were not detected in the separate coculture system.[47] These results suggest that direct penetration induce the important mechanisms for the cell-to-cell transmission of pathogenic α-syn. Our study found that the direct penetration through TNT connections was an important mechanism for intercellular α-syn PFF spreading from BMVECs to pericytes. Although we could not detect significant α-syn PFF transmission in separated cocultures, the barrier function of endothelial cells may obstruct this spreading, as cocultures separated by transwell membranes cannot perfectly imitate the indirect cell-to-cell contacts under physiological conditions. Therefore, the other mechanisms of α-syn PFF transmission from BMVECs to pericytes need to be further studied. Furthermore, the molecular mechanisms of TNT formation are poorly understood.[49] TNT formation between the astrocytes can be induced by intracellular accumulation of α-syn.[23] Microglia exposed to α-syn promoted F-actin-dependent intercellular connections, inhibited Rho-kinase ROCK, a key cytoskeleton regulator and impaired α-syn transfer.[47] In our study, the number of TNTs in the α-syn PFF-treated group was not significantly different from that in the control group. Hence, we consider that the mechanisms of increasing α-syn PFF transfer may not promote TNT formation but may instead activate transport cellular components.

TNTs may contain actin-based myosin motors that mediate actomyosin-dependent transport of endocytic vesicles.[50] The molecular motor myosin-X increases the number of TNTs and the transfer of vesicles between neuronal CAD cells.[51] To confirm the subtype of myosin motors in α-syn PFF-treated BMVECs, we used RNA-seq and screened Myo1d on the basis of DEGs and GO terms. Myo1d colocalizes with F-actin in the dendritic spines of primary hippocampal neurons and the myelin-like membrane edge of oligodendrocytes.[52,53] Myo1d may contribute to membrane dynamics in the transport of myelin membrane proteins during myelination.[54] Here, we demonstrated that α-syn PFF treatment can obviously upregulate Myo1d expression and its colocalization with F-actin. Myo1d siRNA treatment decreased α-syn PFF transmission from BMVECs to pericytes. We further analyzed the difference in the reduction in transmission efficiency after latrunculin B and Myo1d siRNA treatment and found a difference of approximately 5%. Kittelberger, N. et al. found that class 1 myosin motors affected exocytosis as possible linkers between actin and membranes, and the inhibition of myosin 1c reduced exocytosis.[55] Consequently, we speculate that the decrease in transmission efficiency after Myo1d siRNA treatment compared with latrunculin B treatment was caused by alterations in exocytosis due to inhibition of Myo1d. In addition, we unexpectedly found that the transmission efficiency of α-syn PFF significantly decreased under low-glucose culture conditions. Myosin motors move along actin filaments through the use of energy produced by ATP hydrolysis[56]; however, low-glucose medium can reduce ATP production and cause myosin dysfunction, further diminishing the transmission efficiency of α-syn PFF. Based on these findings, Myo1d activation by α-syn PFF in BMVECs promotes α-syn PFF spreading to pericytes.

This study is the first to highlight the TNT and myosin-related mechanisms by which α-syn PFF spread from BMVECs to pericytes. Accordingly, α-syn PFF in BMVECs has the highest transmission efficiency to pericytes. TNT connections between BMVECs and pericytes are important for intercellular α-syn PFF spreading. The mechanisms underlying increased α-syn PFF transfer may not promote TNT formation, but instead may activate the molecular motor Myo1d. Pharmacologically inhibiting Myo1d expression reduces α-syn PFF spread to pericytes; thus, targeting Myo1d may be a promising approach for preventing α-syn spreading from the blood to the brain.

Limitations of the study

In this study, we demonstrated that TNT connections between BMVECs and pericytes were responsible for α-syn PFF transmission, however, we did not rule out other transmission mechanisms. Our study suggests that Myo1d is a key molecule in the spread of α-syn PFFs from BMVECs to pericytes and may be a pharmacological target in preventing α-syn spreading from the blood to the brain, but the role for Myo1d in α-syn PFF transmission needs to be further studied to investigate whether specific knockdown of Myo1d in mouse BMVECs can prevent α-syn spreading from the blood to the brain.

STAR★METHODS

Detailed methods are provided in the online version of this paper and include the following:

- KEY RESOURCES TABLE
- RESOURCE AVAILABILITY
  - Lead contact
  - Materials availability
  - Data and code availability
- EXPERIMENTAL MODEL AND SUBJECT DETAILS
  - Isolation of BMVECs, pericytes and astrocytes
- METHOD DETAILS
  - α-syn PFF generation and labeling
  - Quantification of α-syn PFF transfer in coculture systems
  - Quantification of TNT-connected cells in coculture systems
  - RNA sequencing
  - siRNA treatment
  - Western blotting
  - Immunofluorescence staining
  - Quantitative real-time PCR
  - Transendothelial electrical resistance (TEER) measurement
  - Permeability assay
  - TEM measurement
  - Thioflavin T assay
  - Flow cytometry assays
- QUANTIFICATION AND STATISTICAL ANALYSIS

SUPPLEMENTAL INFORMATION

Supplemental information can be found online at https://doi.org/10.1016/j.isci.2023.107458.

AUTHOR CONTRIBUTIONS

Q.R.D. and L.J.W. conceived and designed the experiments. Q.R.D., Q.X.Z., K.N., R.H., and J.H.Y. prepared the materials and performed the experiments. Q.R.D., P.K.H., T.Z.H., and H.F.H collected and analyzed the data. Q.R.D. wrote the original draft of the manuscript. Q.R.D., G.X.M., Y.H.Z., Y.Y.G., and L.J.W. reviewed and revised the manuscript. All authors read and approved the final version of the manuscript.

DECLARATION OF INTERESTS

The authors declare no competing interests.

INCLUSION AND DIVERSITY

We support inclusive, diverse, and equitable conduct of research.

REFERENCES

1. Qi, S., Yin, P., Wang, L., Qu, M., Kan, G.L., Zhang, H., Zhang, Q., Xiao, Y., Deng, Y., Dong, Z., et al. (2021). Prevalence of Parkinson's Disease: A Community-Based Study in China. Mov. Disord. 36, 2940–2944. https://doi.org/10.1002/mds.28762.

2. Rocha, E.M., De Miranda, B., and Sanders, L.H. (2018). Alpha-synuclein: Pathology, mitochondrial dysfunction and neuroinflammation in Parkinson's disease. Neurobiol. Dis. 109 (Pt B), 249–257. https://doi.org/10.1016/j.nbd.2017.04.004.

3. Patterson, J.R., Polinski, N.K., Duffy, M.F., Kemp, C.J., Luk, K.C., Volpicelli-Daley, L.A., Kanaan, N.M., and Sortwell, C.E. (2019). Generation of Alpha-Synuclein Preformed Fibrils from Monomers and Use In Vivo. J. Vis. Exp. 148. https://doi.org/10.3791/59758.

4. Wang, B., Underwood, R., Kamath, A., Britain, C., McFerrin, M.B., McLean, P.J., Volpicelli-Daley, L.A., Whitaker, R.H., Placzek, W.J., Becker, K., et al. (2018). 14-3-3 Proteins Reduce Cell-to-Cell Transfer and Propagation of Pathogenic α-Synuclein. J. Neurosci. 38, 8211–8232. https://doi.org/10.1523/jneurosci.1134-18.2018.

5. Polinski, N.K., Volpicelli-Daley, L.A., Sortwell, C.E., Luk, K.C., Cremades, N., Gottler, L.M., Froula, J., Duffy, M.F., Lee, V.M.Y., Martinez, T.N., and Dave, K.D. (2018). Best Practices for Generating and Using Alpha-Synuclein Pre-Formed Fibrils to Model Parkinson's Disease in Rodents. J. Parkinsons Dis. 8, 303–322. https://doi.org/10.3233/jpd-171248.

6. Bernis, M.E., Babila, J.T., Breid, S., Wüsten, K.A., Wüllner, U., and Tamgüney, G. (2015). Prion-like propagation of human brain-derived alpha-synuclein in transgenic mice expressing human wild-type alpha-synuclein. Acta Neuropathol. Commun. 3, 75. https://doi.org/10.1186/s40478-015-0254-7.

7. Luk, K.C., Kehm, V., Carroll, J., Zhang, B., O'Brien, P., Trojanowski, J.Q., and Lee, V.M.Y. (2012). Pathological α-synuclein transmission initiates Parkinson-like neurodegeneration in nontransgenic mice. Science (New York, N.Y.) 338, 949–953. https://doi.org/10.1126/science.1227157.

8. Mabbott, N.A. (2017). How do PrP(Sc) Prions Spread between Host Species, and within Hosts? Pathogens 6, 60. https://doi.org/10.3390/pathogens6040060.

9. Chahine, L.M., Beach, T.G., Brumm, M.C., Adler, C.H., Coffey, C.S., Mosovsky, S., Caspell-Garcia, C., Serrano, G.E., Munoz, D.G., White, C.L., 3rd, et al. (2020). In vivo distribution of α-synuclein in multiple tissues and biofluids in Parkinson disease. Neurology 95, e1267–e1284. https://doi.org/10.1212/wnl.0000000000010404.

10. Lohmann, S., Bernis, M.E., Tachu, B.J., Ziemski, A., Grigoletto, J., and Tamgüney, G. (2019). Oral and intravenous transmission of α-synuclein fibrils to mice. Acta Neuropathol. 138, 515–533. https://doi.org/10.1007/s00401-019-02037-5.

11. Peelaerts, W., Bousset, L., Van der Perren, A., Moskalyuk, A., Pulizzi, R., Giugliano, M., Van den Haute, C., Melki, R., and Baekelandt, V. (2015). α-Synuclein strains cause distinct synucleinopathies after local and systemic administration. Nature 522, 340–344. https://doi.org/10.1038/nature14547.

12. Matsumoto, J., Stewart, T., Sheng, L., Li, N., Bullock, K., Song, N., Shi, M., Banks, W.A., and Zhang, J. (2017). Transmission of α-synuclein-containing erythrocyte-derived extracellular vesicles across the blood-brain barrier via adsorptive mediated transcytosis: another mechanism for initiation and progression of Parkinson's disease? Acta Neuropathol. Commun. 5, 71. https://doi.org/10.1186/s40478-017-0470-4.

13. Ayloo, S., and Gu, C. (2019). Transcytosis at the blood-brain barrier. Curr. Opin. Neurobiol. 57, 32–38. https://doi.org/10.1016/j.conb.2018.12.014.

14. Sui, Y.T., Bullock, K.M., Erickson, M.A., Zhang, J., and Banks, W.A. (2014). Alpha synuclein is transported into and out of the brain by the blood-brain barrier. Peptides 62, 197–202. https://doi.org/10.1016/j.peptides.2014.09.018.

15. Huang, R., Gao, Y., Duan, Q., Zhang, Q., He, P., Chen, J., Ma, G., Wang, L., Zhang, Y., Nie, K., and Wang, L. (2023). Endothelial LRP1-ICD Accelerates Cognition-Associated Alpha-Synuclein Pathology and Neurodegeneration through PARP1 Activation in a Mouse Model of Parkinson's Disease. Mol. Neurobiol. 60, 979–1003. https://doi.org/10.1007/s12035-022-03119-4.

16. Bernard-Patrzynski, F., Lécuyer, M.A., Puscas, I., Boukhatem, I., Charabati, M., Bourbonnière, L., Ramassamy, C., Leclair, G., Prat, A., and Roullin, V.G. (2019). Isolation of endothelial cells, pericytes and astrocytes from mouse brain. PLoS One 14, e0226302. https://doi.org/10.1371/journal.pone.0226302.

17. Ruck, T., Bittner, S., Epping, L., Herrmann, A.M., and Meuth, S.G. (2014). Isolation of primary murine brain microvascular endothelial cells. J. Vis. Exp. 93, e52204. https://doi.org/10.3791/52204.

18. Larochelle, C., Cayrol, R., Kebir, H., Alvarez, J.I., Lécuyer, M.A., Ifergan, I., Viel, É., Bourbonnière, L., Beauseigle, D., Terouz, S., et al. (2012). Melanoma cell adhesion molecule identifies encephalitogenic T lymphocytes and promotes their recruitment to the central nervous system. Brain 135 (Pt 10), 2906–2924. https://doi.org/10.1093/brain/aws212.

19. Nakagawa, S., Deli, M.A., Kawaguchi, H., Shimizudani, T., Shimono, T., Kittel, A., Tanaka, K., and Niwa, M. (2009). A new blood-brain barrier model using primary rat brain endothelial cells, pericytes and astrocytes. Neurochem. Int. 54, 253–263. https://doi.org/10.1016/j.neuint.2008.12.002.

20. Sun, J., Huang, Y., Gong, J., Wang, J., Fan, Y., Cai, J., Wang, Y., Qiu, Y., Wei, Y., Xiong, C., et al. (2020). Transplantation of hPSC-derived pericyte-like cells promotes functional recovery in ischemic stroke mice. Nat. Commun. 11, 5196. https://doi.org/10.1038/s41467-020-19042-y.

21. Ahmad, A., Patel, V., Xiao, J., and Khan, M.M. (2020). The Role of Neurovascular System in Neurodegenerative Diseases. Mol. Neurobiol. 57, 4373–4393. https://doi.org/10.1007/s12035-020-02023-z.

22. Kimura, S., Hase, K., and Ohno, H. (2013). The molecular basis of induction and formation of tunneling nanotubes. Cell Tissue Res. 352, 67–76. https://doi.org/10.1007/s00441-012-1518-1.

23. Rostami, J., Holmqvist, S., Lindström, V., Sigvardson, J., Westermark, G.T., Ingelsson, M., Bergström, J., Roybon, L., and Erlandsson, A. (2017). Human Astrocytes Transfer Aggregated Alpha-Synuclein via Tunneling Nanotubes. J. Neurosci. 37, 11835–11853. https://doi.org/10.1523/jneurosci.0983-17.2017.

24. Abounit, S., Bousset, L., Loria, F., Zhu, S., de Chaumont, F., Pieri, L., Olivo-Marin, J.C., Melki, R., and Zurzolo, C. (2016). Tunneling nanotubes spread fibrillar α-synuclein by intercellular trafficking of lysosomes. EMBO J. 35, 2120–2138. https://doi.org/10.15252/embj.201593411.

25. Dieriks, B.V., Park, T.I.H., Fourie, C., Faull, R.L.M., Dragunow, M., and Curtis, M.A. (2017). α-synuclein transfer through tunneling nanotubes occurs in SH-SY5Y cells and primary brain pericytes from Parkinson's disease patients. Sci. Rep. 7, 42984. https://doi.org/10.1038/srep42984.

26. Abounit, S., and Zurzolo, C. (2012). Wiring through tunneling nanotubes–from electrical

signals to organelle transfer. J. Cell Sci. *125* (Pt 5), 1089–1098. https://doi.org/10.1242/jcs.083279.

27. Cordero Cervantes, D., and Zurzolo, C. (2021). Peering into tunneling nanotubes-The path forward. EMBO J. *40*, e105789. https://doi.org/10.15252/embj.2020105789.

28. Errede, M., Mangieri, D., Longo, G., Girolamo, F., de Trizio, I., Vimercati, A., Serio, G., Frei, K., Perris, R., and Virgintino, D. (2018). Tunneling nanotubes evoke pericyte/ endothelial communication during normal and tumoral angiogenesis. Fluids Barriers CNS *15*, 28. https://doi.org/10.1186/s12987-018-0114-5.

29. Hirokawa, N., Niwa, S., and Tanaka, Y. (2010). Molecular motors in neurons: transport mechanisms and roles in brain function, development, and disease. Neuron *68*, 610–638. https://doi.org/10.1016/j.neuron.2010.09.039.

30. Sun, Y.Y., Bradley, J.M., and Keller, K.E. (2019). Phenotypic and Functional Alterations in Tunneling Nanotubes Formed by Glaucomatous Trabecular Meshwork Cells. Invest. Ophthalmol. Vis. Sci. *60*, 4583–4595. https://doi.org/10.1167/iovs.19-28084.

31. Takaki, R., Mugnai, M.L., and Thirumalai, D. (2022). Information flow, gating, and energetics in dimeric molecular motors. Proc. Natl. Acad. Sci. USA *119*, e2208083119. https://doi.org/10.1073/pnas.2208083119.

32. Hegan, P.S., Ostertag, E., Geurts, A.M., and Mooseker, M.S. (2015). Myosin Id is required for planar cell polarity in ciliated tracheal and ependymal epithelial cells. Cytoskeleton (Hoboken, N.J.) *72*, 503–516. https://doi.org/10.1002/cm.21259.

33. Alam, P., Holst, M.R., Lauritsen, L., Nielsen, J., Nielsen, S.S.E., Jensen, P.H., Brewer, J.R., Otzen, D.E., and Nielsen, M.S. (2022). Polarized α-synuclein trafficking and transcytosis across brain endothelial cells via Rab7-decorated carriers. Fluids Barriers CNS *19*, 37. https://doi.org/10.1186/s12987-022-00334-y.

34. Takami, Y., Wang, C., Nakagami, H., Yamamoto, K., Nozato, Y., Imaizumi, Y., Nagasawa, M., Takeshita, H., Nakajima, T., Takeda, S., et al. (2022). Novel pathophysiological roles of α-synuclein in age-related vascular endothelial dysfunction. FASEB J. *36*, e22555. https://doi.org/10.1096/fj.202101621R.

35. Kuan, W.L., Bennett, N., He, X., Skepper, J.N., Martynyuk, N., Wijeyekoon, R., Moghe, P.V., Williams-Gray, C.H., and Barker, R.A. (2016). α-Synuclein pre-formed fibrils impair tight junction protein expression without affecting cerebral endothelial cell function. Exp. Neurol. *285*, 72–81. https://doi.org/10.1016/j.expneurol.2016.09.003.

36. Bazzoni, G., and Dejana, E. (2004). Endothelial cell-to-cell junctions: molecular organization and role in vascular homeostasis. Physiol. Rev. *84*, 869–901. https://doi.org/10.1152/physrev.00035.2003.

37. Doll, D.N., Hu, H., Sun, J., Lewis, S.E., Simpkins, J.W., and Ren, X. (2015). Mitochondrial crisis in cerebrovascular endothelial cells opens the blood-brain barrier. Stroke *46*, 1681–1689. https://doi.org/10.1161/strokeaha.115.009099.

38. Chen, J., Luo, Y., Hui, H., Cai, T., Huang, H., Yang, F., Feng, J., Zhang, J., and Yan, X. (2017). CD146 coordinates brain endothelial cell-pericyte communication for blood-brain barrier development. Proc. Natl. Acad. Sci. USA *114*, E7622–E7631. https://doi.org/10.1073/pnas.1710848114.

39. Schulz, G.B., Wieland, E., Wüstehube-Lausch, J., Boulday, G., Moll, I., Tournier-Lasserve, E., and Fischer, A. (2015). Cerebral Cavernous Malformation-1 Protein Controls DLL4-Notch3 Signaling Between the Endothelium and Pericytes. Stroke *46*, 1337–1343. https://doi.org/10.1161/strokeaha.114.007512.

40. Dejana, E., Tournier-Lasserve, E., and Weinstein, B.M. (2009). The control of vascular integrity by endothelial cell junctions: molecular basis and pathological implications. Dev. Cell *16*, 209–221. https://doi.org/10.1016/j.devcel.2009.01.004.

41. Charreau, B. (2021). Secretome and Tunneling Nanotubes: A Multilevel Network for Long Range Intercellular Communication between Endothelial Cells and Distant Cells. Int. J. Mol. Sci. *22*, 7971. https://doi.org/10.3390/ijms22157971.

42. Pisani, F., Castagnola, V., Simone, L., Loiacono, F., Svelto, M., and Benfenati, F. (2022). Role of pericytes in blood-brain barrier preservation during ischemia through tunneling nanotubes. Cell Death Dis. *13*, 582. https://doi.org/10.1038/s41419-022-05025-y.

43. Stevenson, T.J., Johnson, R.H., Savistchenko, J., Rustenhoven, J., Woolf, Z., Smyth, L.C.D., Murray, H.C., Faull, R.L.M., Correia, J., Schweder, P., et al. (2022). Pericytes take up and degrade α-synuclein but succumb to apoptosis under cellular stress. Sci. Rep. *12*, 17314. https://doi.org/10.1038/s41598-022-20261-0.

44. Dohgu, S., Takata, F., Matsumoto, J., Kimura, I., Yamauchi, A., and Kataoka, Y. (2019). Monomeric α-synuclein induces blood-brain barrier dysfunction through activated brain pericytes releasing inflammatory mediators in vitro. Microvasc. Res. *124*, 61–66. https://doi.org/10.1016/j.mvr.2019.03.005.

45. Pedicini, L., Miteva, K.T., Hawley, V., Gaunt, H.J., Appleby, H.L., Cubbon, R.M., Marszalek, K., Kearney, M.T., Beech, D.J., and McKeown, L. (2018). Homotypic endothelial nanotubes induced by wheat germ agglutinin and thrombin. Sci. Rep. *8*, 7569. https://doi.org/10.1038/s41598-018-25853-3.

46. Jash, E., Prasad, P., Kumar, N., Sharma, T., Goldman, A., and Sehrawat, S. (2018). Perspective on nanochannels as cellular mediators in different disease conditions. Cell Commun. Signal. *16*, 76. https://doi.org/10.1186/s12964-018-0281-7.

47. Scheiblich, H., Dansokho, C., Mercan, D., Schmidt, S.V., Bousset, L., Wischhof, L., Eikens, F., Odainic, A., Spitzer, J., Griep, A., et al. (2021). Microglia jointly degrade fibrillar alpha-synuclein cargo by distribution through tunneling nanotubes. Cell *184*, 5089–5106.e21. https://doi.org/10.1016/j.cell.2021.09.007.

48. Vargas, J.Y., Loria, F., Wu, Y.J., Córdova, G., Nonaka, T., Bellow, S., Syan, S., Hasegawa, M., van Woerden, G.M., Trollet, C., and Zurzolo, C. (2019). The Wnt/Ca(2+) pathway is involved in interneuronal communication mediated by tunneling nanotubes. EMBO J. *38*, e101230. https://doi.org/10.15252/embj.2018101230.

49. Ljubojevic, N., Henderson, J.M., and Zurzolo, C. (2021). The Ways of Actin: Why Tunneling Nanotubes Are Unique Cell Protrusions. Trends Cell Biol. *31*, 130–142. https://doi.org/10.1016/j.tcb.2020.11.008.

50. Jansens, R.J.J., Tishchenko, A., and Favoreel, H.W. (2020). Bridging the Gap: Virus Long-Distance Spread via Tunneling Nanotubes. J. Virol. *94*, e02120-19. https://doi.org/10.1128/jvi.02120-19.

51. Gousset, K., Marzo, L., Commere, P.H., and Zurzolo, C. (2013). Myo10 is a key regulator of TNT formation in neuronal cells. J. Cell Sci. *126* (Pt 19), 4424–4435. https://doi.org/10.1242/jcs.129239.

52. Koshida, R., Tome, S., and Takei, Y. (2018). Myosin Id localizes in dendritic spines through the tail homology 1 domain. Exp. Cell Res. *367*, 65–72. https://doi.org/10.1016/j.yexcr.2018.03.021.

53. Yamazaki, R., Ishibashi, T., Baba, H., and Yamaguchi, Y. (2016). Knockdown of Unconventional Myosin ID Expression Induced Morphological Change in Oligodendrocytes. ASN neuro *8*, 1759091416669609. https://doi.org/10.1177/1759091416669609.

54. Yamazaki, R., Baba, H., and Yamaguchi, Y. (2018). Unconventional Myosin ID Is Involved in Remyelination After Cuprizone-Induced Demyelination. Neurochem. Res. *43*, 195–204. https://doi.org/10.1007/s11064-017-2413-7.

55. Kittelberger, N., Breunig, M., Martin, R., Knölker, H.J., and Miklavc, P. (2016). The role of myosin 1c and myosin 1b in surfactant exocytosis. J. Cell Sci. *129*, 1685–1696. https://doi.org/10.1242/jcs.181313.

56. Kneussel, M., and Wagner, W. (2013). Myosin motors at neuronal synapses: drivers of membrane transport and actin dynamics. Nat. Rev. Neurosci. *14*, 233–247. https://doi.org/10.1038/nrn3445.

STAR★METHODS

KEY RESOURCES TABLE

REAGENT or RESOURCE	SOURCE	IDENTIFIER
Antibodies		
Myosin Id antibody (H-1)	Santa Cruz Biotechnology	Cat# sc-515292
β-Actin (13E5) Rabbit mAb	Cell Signaling Technology	Cat# 4970
Anti-rabbit IgG, HRP-linked Antibody	Cell Signaling Technology	Cat# 7074
Rabbit monoclonal [EPR17260-263] to CD31	Abcam	Cat# ab222783
Rabbit monoclonal [EPR20992] to Occludin	Abcam	Cat# ab216327
Rabbit monoclonal [EPR7583] to Claudin 5	Abcam	Cat# ab131259
Rabbit monoclonal [BLR092G] to ZO1	Abcam	Cat# ab 276131
CD140b (PDGFRB) Monoclonal Antibody (APB5)	Invitrogen	Cat# 14-1402-82
GFAP Antibody (5C10)	Novus	Cat# NBP1-05197
Goat Anti-Rabbit IgG Alexa Fluor® 555	Abcam	Cat# ab150078
Goat Anti-mouse IgG Alexa Fluor®488	Abcam	Cat# ab150113
Chemicals, peptides, and recombinant proteins		
Dulbecco's Modified Eagle's Medium	GIBCO by Thermo Fisher Scientific	Cat# C11995500BT
Phosphate-Buffered Saline	GIBCO by Thermo Fisher Scientific	Cat# C10010500BT
Type II collagenase	Sigma-Aldrich	Cat# C2-BIOC
type I DNase	Sigma-Aldrich	Cat# 10104159001
ENDOTHELIAL CELL MEDIUM	ScienCell	Cat# 1001
Fetal Bovine Serum	GIBCO by Thermo Fisher Scientific	Cat# 10099141C
Insulin-transferrin-sodium selenite	Sigma-Aldrich	Cat# I3146
smooth muscle growth supplement	ScienCell	Cat# 1152
0.25% trypsin-EDTA	GIBCO by Thermo Fisher Scientific	Cat# 25200056
Human Alpha-synuclein monomer	Proteos	Cat# RP-003
Alexa Fluor® 647 Succinimidyl Esters (NHS esters)	Invitrogen	Cat# A20173
CellTracker™ Green CMFDA	Invitrogen	Cat# C2925
wheat germ agglutinin (WGA) Alexa Fluor®555 conjugate	Invitrogen	Cat# W32464
Latrunculin B	Abcam	Cat# ab144291
LIFE TRIzol Reagent	Thermo Fisher Scientific	Cat# 15596-026
Myo1d siRNA	Santa Cruz Biotechnology	Cat# sc-44609
Control siRNA	Santa Cruz Biotechnology	Cat# sc-37007
siRNA Transfection Medium	Santa Cruz Biotechnology	Cat# sc-36868
siRNA Transfection Reagent	Santa Cruz Biotechnology	Cat# sc-29528
RIPA Lysis Buffer	MedChemExpress	Cat# HY-K1001
Phosphatase inhibitor cocktail	MedChemExpress	Cat# HY-K0021
Protease inhibitor cocktail	MedChemExpress	Cat# HY-K0010
Clarity™ Western ECL Substrate	Bio-Rad	Cat# 1705060
Phalloidin-iFluor 488 Reagent	Abcam	Cat# ab176753
PrimeScript IV 1st strand cDNA Synthesis Mix	Takara	Cat# 6215A
TB Green Fast qPCR Mix	Takara	Cat# RR430A
Transwell membranes	Sigma-Aldrich	Cat# CLS3470
Fluorescein isothiocyanate-dextran	Sigma-Aldrich	Cat# FD40

Continued

REAGENT or RESOURCE	SOURCE	IDENTIFIER
Thioflavin T	MedChemExpress	Cat# HY-D0218
BD Cytofix/Cytoperm™ Fixation and Permeabilization Solution	BD Biosciences	Cat# 554722
Critical commercial assays		
BCA Protein Assay Kit	Beyotime	Cat# P0012
Deposited data		
NCBI Datasets	https://www.ncbi.nlm.nih.gov/	NCBI accession number: PRJNA953083
Experimental models: Cell lines		
Primary BMVEC cells	This paper	N/A
Primary pericyte cells	This paper	N/A
Primary astrocyte cells	This paper	N/A
Oligonucleotides		
Myo1d primer for 5'HA (Forward) brp_5HA_FOR: GTGGTTAAGCTGTTCGCCTTG	This paper	N/A
Myo1d primer for 5'HA (Reverse) brp_5HA_REV: GCCTTGAGCATGATGGCAA	This paper	N/A
Gapdh primer for 5'HA (Forward) brp_5HA_FOR: TTGATGGCAACAATCTCCAC	This paper	N/A
Gapdh primer for 5'HA (Reverse) brp_5HA_REV: CGTCCCGTAGACAAAATGGT	This paper	N/A
Software and algorithms		
IBM SPSS Statistics	IBM Software.	https://www.ibm.com/products/spss-statistics
GraphPad Prism 9	GraphPad Software. Inc.	https://www.graphpad.com/
ImageJ (Fiji)	NIH	https://imagej.nih.gov/ij/
Dr.Tom system	Beijing Genomics Institute	https://biosys.bgi.com/
Other		
Leica TCS SP8 STED	Leica	equipment
7500 Real-Time PCR System	ABI	equipment
Millicell ERS-2 electrical resistance system	Merck Millipore	equipment
BD FACSAria flow cytometer	BD Biosciences	equipment

RESOURCE AVAILABILITY

Lead contact

Further information and requests for resources and reagents should be directed to and will be fulfilled by the lead contact, Lijuan Wang (wanglijuan@gdph.org.cn).

Materials availability

This study did not generate new unique reagents.

Data and code availability

- RNA sequencing data have been deposited in the NCBI Sequence Read Archive (SRA) repository under project PRJNA953083. Accession numbers are listed in the key resources table.

- This paper does not report original code.

- Any additional information required to reanalyze the data reported in this paper is available from the lead contact upon request.

EXPERIMENTAL MODEL AND SUBJECT DETAILS

Primary BMVEC, pericyte and astrocyte cells were isolated from C57BL/6 mice (wild-type, postnatal day 1-3) brains. Primary cultures were incubated at 37°C with 5% CO_2.

Isolation of BMVECs, pericytes and astrocytes

BMVECs were isolated according to the method of (Ruck, T.et al., 2014).[17] BMVECs were isolated from postnatal day 1-3 C57BL/6 mouse cortical tissue. The brain was separated into two hemispheres and cut between the cerebellum and the midbrain. The meninges were removed from the two hemispheres under a dissection microscope. The meninges-free forebrains were transferred to DMEM, and the tissue was minced with a pipette. The tissue was then digested with DMEM containing 1.05 mg/mL type II collagenase and 58.5 U/mL type I DNase for 60 min at 37°C on an orbital shaker at 150 rpm. The reaction was stopped by adding 10 ml DMEM and centrifuging the cells at 800 × g for 8 min at 4°C. The supernatant was discarded, and the myelin was removed by resuspension in DMEM containing 20% FBS and centrifugation at 1,000 × g for 20 min at 4°C. The upper myelin layer was discarded, and the pellet was resuspended in DMEM with 1 mg/mL collagenase/dispase and 39 U/mL type I DNase for 60 min at 37°C on an orbital shaker at 150 rpm. DMEM was added to the digested cell suspension, and then the resuspended cells were applied to a Percoll gradient and centrifuged at 700 × g for 10 min at 4°C. The microvessel layer on the bottom of the ultracentrifuge tube was collected and washed with DMEM by centrifugation. Brain microvessels were then seeded in a sterile incubator in endothelial cell medium (ScienCell, 1001) at 37°C and 5% CO_2. The medium was changed every two to three days. The cells were split cells when they reached 90-95% confluence using 0.25% trypsin-EDTA. The seeded microvessel cells were labeled as passage 0 (P0) BMVECs, and the passage number was increased by one after each trypsinization. BMVECs were treated with Alexa 647-labeled α-syn PFF for 24 h, and the presence of exogenous α-syn PFF in the BMVECs was confirmed.

Pericytes were isolated from neonatal mouse brains, and the meninges were removed under a dissection microscope. The brains were mechanically minced with a pipette, and the homogenate was digested in DMEM containing 1.05 mg/mL type II collagenase and 58.5 U/mL type I DNase for 10 min at room temperature. Then, the reaction was stopped by adding DMEM and centrifuging the cells at 800 × g for 8 min at 4°C. The resuspended cells were transferred to T25 flasks in low-glucose DMEM supplemented with 20% FBS, 1x penicillin/streptomycin, ITS (42 μg/mL insulin/38 μg/mL Transferrin/50 ng/mL sodium selenite supplement), 100 μg/ mL heparin and 1x smooth muscle growth supplement. Half of the medium volume was changed every other day. The cells were trypsinized using 0.25% trypsin/EDTA and resuspended in fresh medium. Then, the cell suspension was stored in a T25 flask to settle for 1 h. Adherent cells were discarded, and the cell suspension was moved to a new flask. This digestion process was repeated three times. Pericyte purity was then checked by immunostaining.

For the isolation of astrocytes from neonatal mouse cortices, the meninges were removed under a dissection microscope. The cortices were mechanically minced with a pipette and centrifuged (800 g, 8min, 4°C). Then, the homogenate was digested in DMEM containing 1.05 mg/mL type II collagenase and 58.5 U/mL type I DNase for 10 min. The reaction was stopped by adding DMEM and centrifuged (800 g, 8 min, 4°C). The cell suspension was incubated in T75 flasks and cultured in DMEM supplemented with 10% FBS and penicillin/streptomycin (1×). Cells were split at 90-95% confluence using 0.25% trypsin-EDTA.

METHOD DETAILS

α-syn PFF generation and labeling

Recombinant human α-syn monomers were produced from purified α-syn monomers (RP-003, Proteos, USA) by the method of Michael J. Fox Parkinson's Research Foundation.[5] Briefly, α-syn monomers (5 mg/mL diluted in sterile PBS) were incubated at 37°C with agitation in a microplate shaker at 1000 rpm for seven days to form fibrils. Basic quality control experiments were performed to ensure that α-syn monomers successfully aggregated into fibrils, including a thioflavin T assay to assess amyloid fibril structure, transmission electron microscopy (TEM) to determine fibril size and morphology, and Western blotting to assess fibril size. α-Syn PFFs were diluted in PBS and sonicated using an ultrasonic cell disruptor (SCIENTZ-IID) at high intensity for 60 pulses (1 s on; 1 s off).

α-Syn PFFs were labeled with Fluorescent Protein Labeling Kits (Invitrogen, A20173) to obtain Alexa 647-labeled α-syn PFF. Briefly, α-syn PFFs were diluted to 2 mg/mL in PBS, and then 50 μl of a 1 M solution

of sodium bicarbonate was added. The protein solution was transferred to a vial containing the reactive dye, and the reaction mixture was stirred for 1 hour at room temperature.

Quantification of α-syn PFF transfer in coculture systems

Different coculture systems were used to study the cell-to-cell transfer of α-syn PFF. Acceptor cells were stained with CellTracker™ Green CMFDA (5-chloromethylfluorescein diacetate) (Invitrogen, C2925). Briefly, acceptor cells were incubated for 30 min at 37°C with 1 μM CellTracker™ Green (CTG) diluted in serum-free medium. Donor BMVECs were treated with Alexa 647-labeled α-syn PFF for 24 h, and were subsequently washed using PBS. Alexa 647-labeled BSA was administered to the control group. After labeling, donor and acceptor cells were detached, and counted, diluted to a concentration of 22,500 cells/cm^2, replated at a 1:1 ratio in a new plate, and cultured for 72h. Acceptor cells included BMVECs, pericytes and astrocytes; the cells were divided into the BMVEC-to-BMVEC (B-B), BMVEC-to-pericyte (B-P) and BMVEC-to-astrocyte (B-A) groups. Alexa 647-labeled α-syn PFF in acceptor cells were counted, and the data were analyzed using one-way ANOVA statistical analysis.

Quantification of TNT-connected cells in coculture systems

Cells in coculture systems were fixed for 15 min in 4% paraformaldehyde (PFA) and were washed in PBS. Then, the cells were labeled for 20 min at 37°C with a 1:200 solution of wheat germ agglutinin (WGA) Alexa Fluor®555 conjugate (Invitrogen, W32464) in PBS. After additional washes, cells were embedded with DAPI. The TNT-connected cells were imaged by inverted confocal microscopy (Leica). TNT-connected cells with straight WGA-labeled structures were identified by scanning. The connected TNT were counted when they fit the following criteria: protrusions thinner than 1 μm and protrusions with a length of 5-100 μm connecting two cells. For analysis, TNTs were stained with WGA and measurements were performed as previously described.[23] The inclusion criterion for TNTs herein was protrusions connecting two cells with a length of 5-100 μm. Four independent experiments were performed, and 180-250 individual cells were analyzed in each experiment. The number of TNTs was determined manually, and the data are presented as the percentage of TNT-connected cells (number of TNT-connected cells divided by the total number of cells). Actin polymerization was inhibited using 3 μM latrunculin B (abcam, ab144291) 3 h after coculture initiation.

RNA sequencing

Total RNA was extracted from primary BMVECs (1×10^7 cells per sample) treated with PBS and α-syn PFF using TRIzol. The RNA concentration was determined for each sample and the RIN/RON ratio and the 28/18S ratio were assessed using a Fragment Analyzer to confirm that the RNA samples were of sufficient quality for cDNA library construction and sequencing. RNA sequencing was performed using the BGISEQ platform with paired-end 150 bp reads by Beijing Genomics Institute (BGI). After data filtering, 95.55% of the reads were mapped to the genome of *Mus_musculus* genome (NCBI, GCF_000001635.26_GRCm38.p6). A total of 4895 differentially expressed genes (DEGs) were identified using DESeq2 with a Q value ≤ 0.05. Kyoto Encyclopedia of Genes and Genomes (KEGG) pathway analysis and Gene Ontology (GO) enrichment analysis were performed using the Dr.Tom system developed by BGI Genomics.

siRNA treatment

Myo1d siRNA for inhibiting Myo1d expression in mouse cells was purchased from Santa Cruz Biotechnology (sc-44609). Scramble siRNA (Santa Cruz Biotechnology, sc-37007) was used as a control. BMVECs were seeded in 6-well plates in 2 ml antibiotic-free endothelial cell medium until 60-80% confluent. For each transfection, 0.75 μg siRNA was added to 100 μl siRNA Transfection Medium (Santa Cruz Biotechnology, sc-36868), and then mixed with 6 μl of siRNA Transfection Reagent (Santa Cruz Biotechnology, sc-29528) diluted in siRNA Transfection Medium. The cells were washed once with 2 ml of siRNA Transfection Medium, and then a mixture of 0.8 ml siRNA Transfection Medium and 0.2 ml siRNA Transfection Reagent mixture was added. Then, 1 ml endothelial cell medium containing 2× normal serum was added, and the cells were incubated for an additional 20 hours. The medium was replaced with fresh endothelial cell medium, and the cells were incubated for another 48 hours before being assayed by Western blotting.

Western blotting

Cells were lysed with RIPA buffer (MCE, HY-K1001) containing phosphatase inhibitor cocktail (MCE, HY-K0021) and protease inhibitor cocktail (MCE, HY-K0010), and centrifuged at 12,000 × g for 15 min at 4°C. The supernatants were collected, and the protein concentration was tested using a BCA kit (P0012, Beyotime). The protein samples were separated by SDS-PAGE and transferred to PVDF membranes. The membranes were blocked with 5% nonfat milk in TBST for 2h at RT, and incubated with primary and secondary antibodies. The antibodies used were as follows: anti-Myosin ld (1:100, Santa Cruz Biotechnology, sc-515292), anti-β-actin (1:1000, Cell Signaling Technology, 4970), and HRP-linked secondary antibodies (1:10,000, Cell Signaling Technology). The membranes were visualized with a Clarity™ Western ECL Substrate (Bio-Rad, 1705060) and quantitative analysis was conducted using ImageJ. Each target protein level was normalized to that of β-actin. The mean gray value of 3 bands was statistically analyzed in each experiment, and 6 independent experiments were performed (n=6).

Immunofluorescence staining

Cells were washed with PBS three times, fixed for 15 min in 4% PFA, permeabilized with 0.5% Triton X-100 for 15 min, blocked in 10% goat serum for 1 h at RT, and incubated with primary antibodies overnight at 4°C. The primary antibodies used were as follows: anti-Myosin ld (1:100, Santa Cruz Biotechnology, sc-515292), anti-CD31 (1:100, abcam, ab222783), anti-Occludin (1:100, abcam, ab216327), anti-Claudin-5 (1:100, abcam, ab131259), anti-ZO-1 (1:100, abcam, ab276131), anti-PDGFR-β (1:200, Invitrogen, 14-1402-82), and anti-GFAP (1:100, Novus, NBP1-05197). The following day, the cells were incubated with secondary antibodies for 1 h at RT. The secondary antibodies used were as follows: Goat Anti-Rabbit IgG Alexa Fluor® 555 (1:1000, abcam, ab150078) and Goat Anti-mouse IgG Alexa Fluor®488 (1:1000, abcam, ab150113). After washing, the cells were incubated with DAPI or Phalloidin-iFluor 488 Reagent (1:1000, abcam, ab176753) for 15 min at RT. Images were captured using a LEICA TCS SP8 laser scanning confocal microscope. Colocalization analysis of Myo1d and F-actin was performed using Fiji, and Pearson's R-value was calculated to quantify pixel intensity correlations.

Quantitative real-time PCR

Total RNA was extracted from BMVECs using a TRIzol Plus RNA Purification Kit (Invitrogen). The isolated total RNA was reverse transcribed into cDNA with PrimeScript IV 1st strand cDNA Synthesis Mix (Takara, 6215A). The qPCRs were performed in a 7500 Real-Time PCR System (ABI, USA) using TB Green Fast qPCR Mix (Takara, RR430A). The relative gene expression levels were calculated with the $2^{-\Delta\Delta Ct}$ method using glyceraldehyde-3-phosphate dehydrogenase (Gapdh) as an internal control. Myo1d and Gapdh cDNA were amplified by qPCR with the following primer sets:

Myo1d forward; 5'-GTGGTTAAGCTGTTCGCCTTG-3'

Myo1d reverse; 5'-GCCTTGAGCATGATGGCAA-3'

Gapdh forward; 5'- TTGATGGCAACAATCTCCAC-3'

Gapdh reverse; 5'- CGTCCCGTAGACAAAATGGT-3'

Transendothelial electrical resistance (TEER) measurement

The TEER values of *in vitro* BBB models consisting of BMVEC monocultures, cocultures of BMVECs and pericytes and cocultures of BMVECs, pericytes and astrocytes were measured. Astrocytes (1.5×10^5 cells per well) were seeded in the bottom of the 24-well-plate Transwell membranes (0.4 μm pore size, CLS3470, Sigma-Aldrich) and incubated overnight. Pericytes (4.5×10^4 cells per well) were plated on the basal side of the membrane for 24 h. Then, BMVECs were trypsinized and seeded on the apical side of the Transwell inserts at a density of 6.4×10^4 cells per well. α-Syn PFFs were added to the apical side and treated BMVECs. TEER measurements were obtained after endothelial cell seeding using the Millicell ERS-2 electrical resistance system (MERS00002, Merck Millipore).[35]

Permeability assay

Permeability was measured by the method of (Doll, D. N. et al., 2015)[37] using fluorescein isothiocyanate-dextran (FD40, 40,000 MW, Sigma-Aldrich). BMVECs, pericytes and astrocytes were used for the *in vitro*

BBB model. Medium containing 2.5 mg/mL FD40 was added to the upper compartment, and that in the basal compartment was replaced with 400 μL of fresh medium. Every 10 min, 50 μL of medium in the basal compartment was collected and replaced with fresh medium. The fluorescence of the collected samples was measured using a microplate reader (Thermo Fisher Scientific, USA) under 485 nm excitation/ 520 nm emission.

TEM measurement

Unsonicated and sonicated α-syn PFFs were adsorbed on carbon-coated 200-mesh copper grids for 2 min at RT and negatively stained with 3% phosphotungstic acid (pH 7.0) for 2 min at RT. Distilled water was gently dripped onto the copper grids, which were then dried for several minutes. Images were acquired using a Philips CM 10 electron microscope operated at 80 kV.

Thioflavin T assay

The thioflavin T assay was performed by the method of (Patterson, J. R. et al., 2019).[3] Five microliters of α-syn monomers or α-syn PFFs were added to 245 μL of PBS, mixed with 250 μL of thioflavin T (25 μM thioflavin T, MCE, HY-D0218) in a 96-well plate, and then incubated for 30 min at 37°C in the dark. The fluorescence intensity of thioflavin T was measured using a microplate reader (Thermo Fisher Scientific, USA) at 485 nm excitation/520 nm emission.

Flow cytometry assays

Extracellular and intracellular stainings was performed by the method of (Larochelle, C. et al., 2012).[18] Briefly, isolated BMVECs, pericytes and astrocytes were trypsinized and resuspended in BD Pharmingen™ Stain Buffer (FBS). Cells were incubated with the antibodies against the surface markers CD31 (1:100, Invitrogen, RM5201) and PDGFR-β (1:100, Invitrogen,14-1402-82). For intracellular staining, a GFAP specific antibody (1:100, abcam, ab7260) was used to label astrocytes. Intracellular staining was performed using the BD Cytofix/Cytoperm™ Fixation and Permeabilization Solution (554722). Nonspecific background staining was assessed by appropriate fluorochrome-matched isotype antibodies. A BD FACSAria flow cytometer (version 6.1) was used to analyzed cell staining.

QUANTIFICATION AND STATISTICAL ANALYSIS

SPSS (version 26.0 SPSS) was used for the statistical analyses. Data were collected from at least three independent tests. Comparisons between the two groups were made by Student's t test for normally distributed variables and the Mann-Whitney tests for nonnormally distributed variables. One-way ANOVA was used for three or more groups of data. Two-Way Repeated-Measures ANOVA was used for repeatedly measured variables. Bonferroni and Tukey's adjustments were applied to correct the p value in multiple comparisons. Data are presented as the mean±SD. A p value< 0.05 was considered statistically significant.